The Kinetic Studies on Ethane Dehydrogenation Using Carbon Dioxide as Mild Oxidant over Gallium Aluminum Mixed Oxide

by

Hsuan-Lan Wang

A thesis submitted to the Faculty of the University of Delaware in partial fulfillment of the requirements for the degree of Master of Chemical Engineering

Winter 2020

The Kinetic Studies on Ethane Dehydrogenation Using Carbon Dioxide as Mild Oxidant over Gallium Aluminum Mixed Oxide

by

Hsuan-Lan Wang

Approved: _____
Raul F. Lobo, PhD
Professor in charge of thesis on behalf of the Advisory Committee

Approved: _____
Dionisios G. Vlachos, PhD
Professor in charge of thesis on behalf of the Advisory Committee

Approved: _____
Eric M. Furst, PhD
Chair of the Department of Chemical and Biomolecule Engineering

Approved: _____
Levi T. Thompson, PhD
Dean of the College of College Name

Approved: _____
Douglas J. Doren, Ph.D.

Interim Vice Provost for Graduate and Professional Education and Dean of the Graduate College

ACKNOWLEDGMENTS

First of all, I would like to express my sincere appreciation to my advisors, Professor Raul Lobo and Professor Dionisios Vlachos. They gave consistent and patient guidance with their valuable experience. They gave their trusts on students and willingness to lead their students to reach higher achievements.

I want to give many thanks to Dr. Weiqing Zheng, Dr. Hilal Toraman and Dr. Weiqi Chen who have gave me valuable advice and guides on either doing experiments, analyzing data and decision making of research work throughout my laboratory life. I have learned from them how to become a researcher with high sense of responsibility and how to contribute myself in the group to help each other. I would also like to thank the group members from both groups, Sai Praneet, Muyuan Li, Tai-Ying Chen, Mingchun Ye, Eric Steinman, Mark LaFollette, Jason Lee who all have given a hand during the years in University of Delaware.

I want to thank my dear roommates, Yu-Ching Kao and Jialiu Jiang, who have been there from the very beginning of the journey and always show their supports and cares. The happiness I received through the life living with them is one of the strongest encouragements in the long period of tough time. Many thanks also go to all my friends from Taiwanese Students Association in University of Delaware, who have brought so much joy to me in my graduate life.

Last but not least, I want to thank my parents who are always my strongest support and trust me without any doubt. They take care of whichever side of me, happy or sad, bright or dark, vigorous or depressed. Without knowing that they are always there and accept whoever I would become. I would not have gone this far to make it.

TABLE OF CONTENTS

LIST OF TABLES

LIST OF FIGURES

ABSTRACT

The development of a stable catalyst with high reactivity and selectivity for ethane dehydrogenation has been a long-studied topic in the field of energy research. The synergetic effect of the mixed gallium and aluminum oxide had been identified and received a quantitative evaluation in this work. We identified an optimized composition of the mixed oxide prepared via co-precipitation method at the surface Ga/Al ratio of 0.1 and conducted a series of kinetic measurements on different surface Ga loading. The kinetic parameters are found to be sensitive of the surface composition. The reaction order on ethane is close to 1 for γ-Al_2O_3 and the surface Ga/Al ratio lower than 0.1, while it is close to 0.7 for ratio is above 0.1 and Ga_2O_3. We also evaluate the effects of the utilization of CO2 as the mild oxidant in ethane dehydrogenation. Based on the kinetic experiments as well as the catalyst characterization, we propose that CO_2 does not directly participate into the ethane dehydrogenation. On the other hand, it serves as a mild oxidant oxidizing the carbonaceous components produced via side cracking reactions and extend the lifetime of the catalyst by decelerate the propagation of graphitic coke.

Chapter 1

INTRODUCTION

Light olefins are key building blocks in the chemical industries as the source to synthesize numerous products such as polyethylene, polystyrene and ethylene oxide. Therefore, the production of light olefins has always been a topic receiving great attention. Among hydrocarbons, ethylene is one of the most widely used and can be upgraded into various derivatives. Its end products can go into markets include, but not restricted to, packaging, transportation, electronic, construction and consumer chemicals as well as coating and adhesives.[1], [2] Natural gas liquid (NGL) and naphtha are common feedstock for the ethylene production via thermal cracking or fluid catalytic cracking (FCC). In recent years, the development in the technologies of shale gas utilization has decreased the costs of NGL since shale gas is mainly composed of methane and other minor hydrocarbon such as ethane and propane. Therefore, researches have been focused on developing alternative pathways for ethylene production with higher selectivity and lower energy costs. The catalytic dehydrogenation can meet the above requirements, but productivity and stability remain challenging for the implement of catalytic dehydrogenation in industries.[3] There are non-oxidative and oxidative catalytic dehydrogenation on which the choice of catalysts will be different depends on their active sites. [4], [5]

1.1 Catalytic Ethane Dehydrogenation

Catalytic ethane dehydrogenation (EDH) started with the knowledge of C-H bond activation. From the thermodynamic aspect, the ethane dehydrogenation is a one-step

reaction from paraffins to their corresponding olefins and hydrogen, which requires massive energy intake for the activation of the C-H bond.

$$C_2H_6 \rightarrow C_2H_4 + H_2 \qquad \Delta H^0_{298} = 137\ kJ/mol \tag{R1}$$

Its thermodynamic natures imply that the reaction favors higher operating temperature at lower pressure to reach higher conversion. Typically, temperature of 550-700 ℃ at ambient pressure will be the operating condition for ethane dehydrogenation.[6]–[8] However, at the same condition, hydrogenolysis of alkanes to smaller hydrocarbon, catalytic cracking of olefins.[9] The side reactions will generate the precursors of coke such as methane and other carbonaceous components.[10]–[13] Hence, the poor stability of the catalytic dehydrogenation remains a challenge and efforts have been put on developing catalysts catalyzing less cracking as well as the optimal operating conditions for ethane dehydrogenation. In short, the non-oxidative ethane dehydrogenation would suffer from its thermodynamic limitations on the conversion as well as the trade-off between the activity and stability.

There were two major types of catalysts which are noble metal-based and metal oxide based respectively. Platinum-based catalysts have been the most extensively studied among noble metal-based catalysts.[6], [14]–[16] On the contrary, there are multiple choices have been identified as metal oxide-based catalysts such as chromium, gallium, indium, vanadium, zinc and molybdenum oxide.[11], [14], [17]–[26] The goal of the catalyst development is to find a catalyst with high activity and selectivity to

ethylene production yet able to maintain the stability throughout the reaction. The synthesizing costs and toxicity are also critical criteria towards the catalyst design.

Among variable choices, gallium oxide has been found that meets most of the requirements. Gallium was then deposited on several supports such as Al_2O_3, TiO_2, SiO_2, H-ZSM5 as well as other molecule sieves pursuing better activity as well as selectivity.[9], [27]–[32] Gallium on Al_2O_3 and H-ZSM5 has shown high selectivity towards ethylene (over 85%). Ga/H-ZSM5 has been well studied for the ethane dehydrogenation mechanism. However, the reaction pathway for Ga/Al_2O_3 has yet been well understood. While the natures of the acid sites on Ga/Al_2O_3 has been revealed by Chen *et al*,[33] the role of Ga on the Al_2O_3 and the effect on the activity of the catalysts remain controversial. With different Ga loading, different active sites are expected to be presented on the surface of the catalysts, resulting in different mechanisms. There is also a lack of knowledge on the kinetic parameters of the Ga/Al_2O_3 catalyst. Therefore, in this work, we would like to first understand the mechanism pathway of non-oxidative ethane dehydrogenation on Ga/Al_2O_3 through the measurement of kinetic data and compare with the previous DFT-based model.[34] Through the validation of the model, we could further verify the interaction between Ga and Al and its reflection on the mechanism.

To describe the mechanism of the non-oxidative ethane dehydrogenation, it depends case by case on variable surface of catalysts as well as types of active sites. Nevertheless, it is generally believed that a Langmuir-Hinshelwood model can be used to develop the rate law for the reaction.[35], [36] The C-H activation of ethane is often

identified as the rate determining step for dehydrogenation while the desorption of H_2 is usually the secondary slow step due to its high energy barrier. In this work, we specifically develop rate laws for different targeted catalyst surfaces and discuss the relationship between the active sites with the apparent kinetic parameters by comparing the experimental data with previous computational work.[34]

1.2 Oxidative Ethane Dehydrogenation

One critical problem of using Ga series catalysts is its poor stability. Cracking of the hydrocarbons is a strong side reaction of alkane dehydrogenation, which will generate methane, a precursor to coke. Therefore, the deactivation behavior is significant under the quick built-up of coke. From the perspective of catalyst design, improvement has been made by adding Pt dopant on the Ga/Al_2O_3.[23] To accommodate the poor stability as well as increase the conversion of the reaction, the oxidative dehydrogenation has first been proposed to overcome the thermodynamic limitation. Oxygen is the most typical and available oxidant to accept hydrogen and provide heat to the reaction. Its strong oxidizing power is a plus to oxidize coke formed during the reaction and extend the lifespan of the catalysts.[37], [38] However, oxygen will further react with light olefins products to generate unwanted CO_x through secondary reactions due to its strong oxidizing power, resulting a lower selectivity to ethylene. As an alternative, CO_2 is considered to be a milder oxidant to consume H_2 through reverse water gas shift (R2) and overcome the thermodynamic equilibrium of

the dehydrogenation process.[39], [40] With the higher initio CO_2 to propane ratio, the more olefin equilibrium yield can be reached based on thermodynamic calculation.

$$CO_2 + H_2 \rightarrow CO + H_2O \qquad 41.5 \text{ kJ/mol} \qquad \text{(R2)}$$

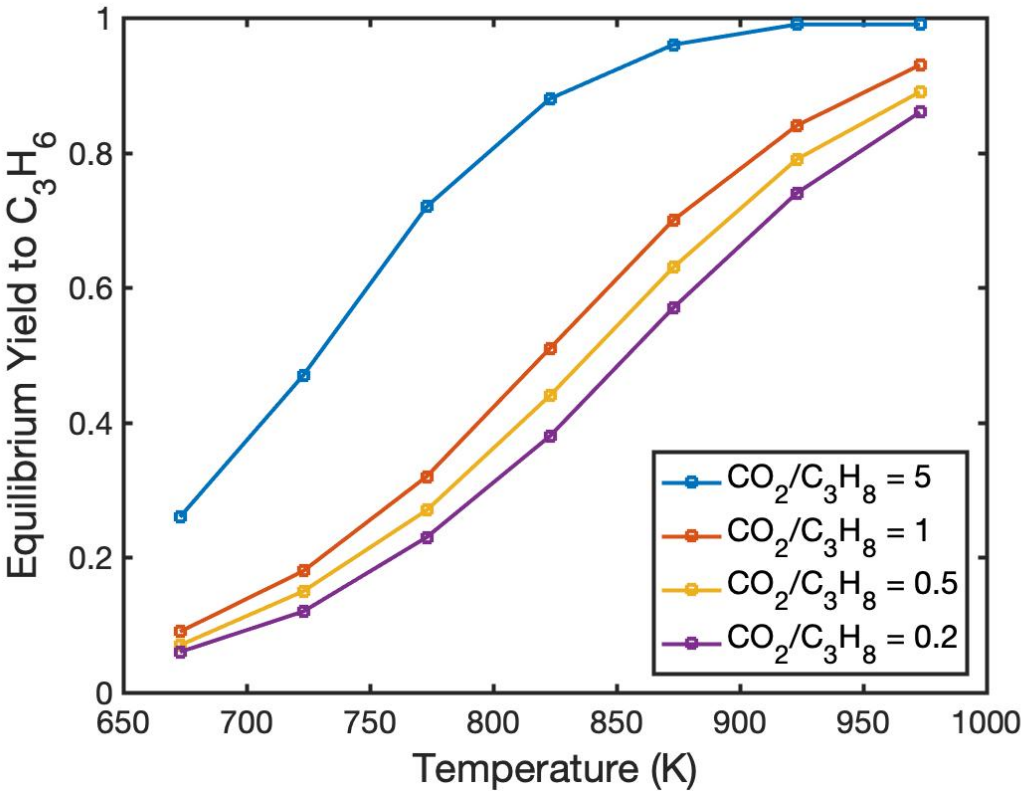

Figure 1: Equilibrium yield to propylene in oxidative propane dehydrogenation using CO_2 as mild oxidant at different level of initial CO_2 to propane ratio.[39]

Besides reverse water gas shift, reverse Boudouard reaction (R3) is another reaction that plays an important role in oxidative dehydrogenation of light alkane. CO_2 can react with the carbonaceous components, which are produced by the unwanted side

cracking reactions, and prevent the fast propagation of coke via reverse Boudouard reaction.

$$C + CO_2 \rightarrow 2CO \qquad 172.5 \text{ kJ/mol} \qquad \text{(R3)}$$

With the use of CO_2, it has been first found by Nakagawa *et al*.[41], [42] that the conversion of ethane can be much improved in the oxidative condition using Ga_2O_3. During 2000s, Xu *et al*.[43] has investigated effects of supports for Ga_2O_3 and Chen *et al*.[33] has looked at the performance of Ga/Al_2O_3 at different levels of Ga loading in oxidative propane dehydrogenation. Yet the effect of CO_2 on the stability of catalysts have not been systematically described. Hence, in this work, we systematically evaluate the effect of carbon dioxide on the activity and stability of the catalysts and identify the change of deactivation behavior in the presence of CO_2.

Chapter 2

EXPERIMENTAL METHODS

2.1 Catalyst Synthesis

A series of gallium and aluminum mixed oxide has been prepared through co-precipitation methods with Ga loading of 0, 6 wt%, 25 wt% and 100 wt%. Appropriate amounts of Gallium (III) nitrate hydrate ($Ga(NO_3)_3 \cdot xH_2O$ 99.9% trace metals basis, Sigma-Aldrich) and aluminum nitrate nonahydrate ($Al(NO_3)_3 \cdot xH_2O$ 99.997% trace metals basis, Sigma-Aldrich) were dissolved in the same bottle of 100 ml deionized water. One hundred milliliter of 1M mixed nitrate solution and excess 1M ammonium carbonate solution were added dropwise into another bottle of 100 ml deionized water at room temperature with vigorous agitation. Solids were precipitated out of solution at this point. The mixture is stirred for another two hours to allow for the mixed oxide to ripe. The whole co-precipitation process was controlled at pH = 8. The molecular structure of the precipitants was not characterized. However, since aluminum and gallium hydroxides have low solubility (their K_{sp} are the order of 10^{-34} and 10^{-36}) ; they are likely the direct precipitates. Moreover, it is possible that gallium hydroxide first precipitate due to the smaller K_{sp}. The precipitate was then collected through centrifugal sedimentation and washed by water for three rounds. The collected sample was dried at 80 ℃ overnight and then calcined at 700 ℃ in air for 8 hr.

The nomenclature of the catalysts is on the basis of the ratio of Al to Ga in the precursor. The catalyst with Al to Ga ratio of *x* is called AxG1. Pure alumina and gallia were prepared through precipitation method and are named AL and GA respectively.

2.2 Characterization

2.2.1 Surface Area Measurement (BET)

The catalyst was first degassed in a heating unit under vacuum at 250 °C for 3 hr to remove water and any adsorbed contamination. The sample was then utilized to obtain nitrogen adsorption isotherm in a 3Flex unit (Micromeritics) and these data were used to obtain the BET parameters.

2.2.2 X-Ray Powder Diffraction (XRD)

A Bruker D-8 diffractometer was used for X-Ray Powder Diffraction measurement. The crystal structure of catalysts was examined using Cu Kα radiation (λ = 1.5418 Å). The X-ray tube and the detector are both rotating to increase the diffraction 2**θ** angle. The increment of 2**θ** is 0.05º and the detector collect the diffracted X-ray for 1 second at every step. The catalysts are grinded into fine powder and uniformly placed on the powder specimen sample holder. The surface of packed sample will be pressed by a glass slide to prevent a rough surface which would diffract the X-ray and reduce the intensity of the signal.

2.2.3 Thermogravimetric Analysis (TGA)

Thermal gravimetric analysis (TGA-DSC, Discovery SDT 650) was used to measure the amount of coke formed during reactions as well as to characterize qualitatively the coke. 10 mg of spent catalysts was placed in an alumina sample holder.

The temperature in the analyzing chamber was ramped from room temperature to 800 °C at a heating rate of 20 ℃/min under air flow at a flow rate of 50 ml/min. The sample weight at 100 °C, assuming that water has been removed from the sample, was taken as initial weight, and any weight lost was calculated based on this initial weight.

2.2.4 X-Rays Photoelectron Spectrometry (XPS)

The X-rays photoelectron spectrometry was used for the analysis of the surface composition of catalysts. The spectra were collected both before and after the ethane dehydrogenation to evaluate the structure of coke. Measurements were carried out using a Thermo Scientific K-Alpha spectrometer equipped with a monochromator and a 128 channel CCD detector plate. The X-rays source was monochromatic Al Kα X-rays (1486.7 eV) with a power of 72W (12 kV, 6mA). The beam shape and size of X-rays was elliptical and roughly 400 μm. The sample powder was first pressed into a tablet to ensure only the catalyst is exposed to the X-rays beam. The survey scan was first collected at a pass energy of 50 eV with step size of 1.0 eV. High-resolution spectra were collected for Al2p, Ga3d, Ga2p, C1s and O1s at a pass energy of 20 eV with step size of 0.1 eV.

CasaXPS was used to deconvolute the spectra and quantify the atomic ratio on the surface of catalysts. The Shirley type background was applied, and the binding energy was calibrated to the C1s sp3 peak at 284.8 eV. The C1s sp2 spectrum was fitted with Doniach-Sunjic convoluted with Gaussian-Laurenzo functions due to its asymmetric shape. Other symmetric peaks were all fitted with Gaussian-Laurenzo profile.

2.2.5 Solid-State Nuclear Magnetic Resonance (NMR) Spectroscopy

The ^{27}Al Magic Angle Spinning **N**uclear Magnetic Resonance (MAS NMR) spectra were collected on a Bruker AVIII 500 MHz solid-state NMR spectrometer with a 4mm HX probe at a spinning speed of 12 kHz and a frequency of 130.312 MHz. ^{27}Al spectra were acquired with a 1.7 μs pulse length and a 1 s pulse delay. For all spectra 1024 scans were acquired.

2.3 Catalyst Reactivity

The catalysts were tested under both non-oxidative and oxidative (CO_2) ethane dehydrogenation conditions. The reaction takes place in a plug flow quartz reactor with a 7 mm inside diameter at atmospheric pressure. The setup of the flow system is depicted in Figure 2. Total 200 mg of catalysts are pressed into a pellet under high pressure. The pellet was then grinded and sieved. Sieved catalyst particles with a diameter in the range of 250 to 425 μm are collected for reactivity and stability tests. The catalyst bed is ~1 cm long consisting of 80 mg catalyst and 200 mg of quartz chips which are made of the wasted quartz reactor to assure the same heat expansion coefficient as that of the quartz reactor. Another 1.5 cm of quartz chips were packed on top and under the catalyst bed respectively to pre-stabilize the reactant flow and temperature for the central catalyst bed.

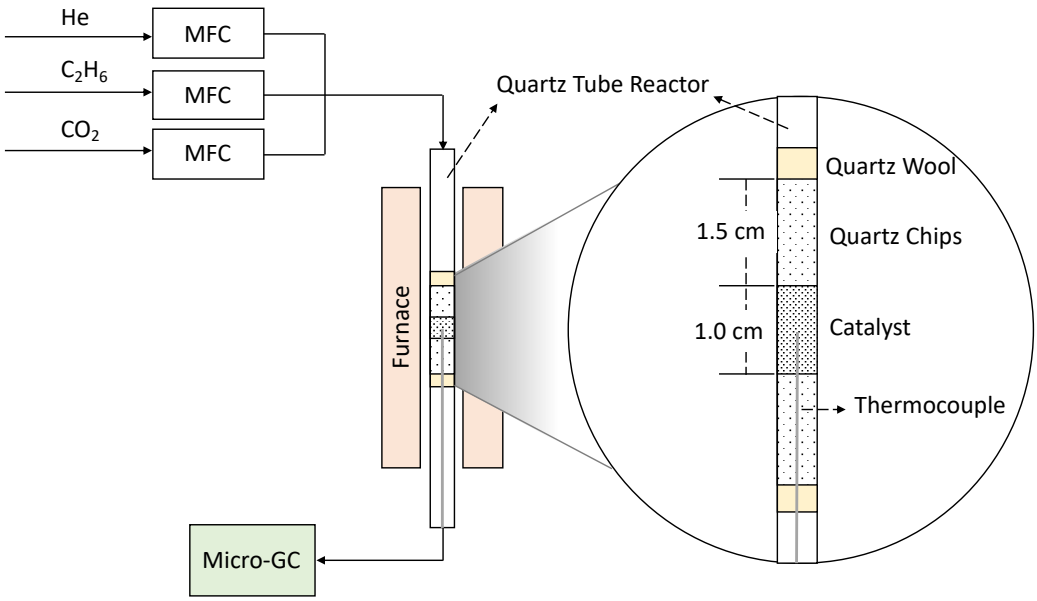

Figure 2: The experimental setup of the packed bed catalytic reactor.

The quartz tube reactor was mounted in a tube furnace (Thermo Scientific Lindberg Blue M) with a K-type thermocouple (Omega Engineering) inserted into the center of catalyst bed to measure the central bed temperature. The reaction mixture consists of ethane (Matheson, purity >99.5%), carbon dioxide (Matheson) and helium (Ultra high purity, 99.999%) as balance gas. The flow rate of each species is controlled by the mass flow controller (MKS Instruments). A micro-GC (Agilent 490) equipped with thermal conductivity detector (TCD) and a mass spectrometer are installed to analyzed effluent composition. In the micro-GC, four columns are used for analyzing different components:

1. a MS5A column with argon (Ar) as carrier gas to measure the components including helium (He), nitrogen (N_2), and hydrogen (H_2),
2. a MS5A column with He as carrier gas to measure the concentration of carbon monoxide (CO),
3. a PPU column with He as carrier gas to measure components including methane (CH_4), CO_2, ethylene (C_2H_4) as well as ethane (C_2H_6), and
4. a Al/KCl column with He as carrier gas for the measurement of other hydrocarbon components.

The investigation for catalyst reactivity is carried out at 600 °C and 1 atm. The catalyst bed is first pretreated by 50 ml/min He at room temperature. The temperature was then ramped to 600 °C at a heating rate of 10 °C/min and then held constant after it reached 600 °C. The reactant mixture is then fed into the reactor. To minimize the effect of gas phase chemistry, the conversion of the reaction has also been measured when there is only an empty quartz tube.

2.4 Kinetic Measurements

The kinetic information for non-oxidative and oxidative (CO_2) ethane dehydrogenation were obtained from the catalytic tests as described above. The apparent reaction orders on ethane and CO_2 were determined within the range of 3.6 kPa to 10 kPa for both ethane and CO_2. The apparent activation energy was obtained within the temperatures of 550 °C to 625°C. The reaction rate with 3.6 kPa of ethane and 3.6 kPa of CO_2 at 600 ℃ is designated as the “standard” level of the activity. To eliminate any

effects from catalyst deactivation, the catalyst sample is regenerated in air every time after a reaction. To this end, air was fed into the reactor at the reaction temperature to regenerate the catalyst, and the burning of coke was monitored by observing the concentration of CO_2 via mass spectrometry (MS). However, regeneration in air can only recover active sites initially covered by coke, but deactivation caused by sintering is irreversible and cannot be recovered. The standard level of activity is used as reference to exclude deactivation by sources other than coking. After regeneration, reaction rates at the standard compositions and temperature are repeated to quantify any effects of irreversible deactivation.

2.5 Conversion and Rate

The conversion of the reaction is calculated based on the inlet and the outlet concentration of ethane. The conversion of the reaction is low enough so that we can assume the reaction is taking place in the differential condition. The initial concentration of the ethane is below 10 mol% and we assume that there is no change in volumetric flow rate throughout reaction. The calculations of the conversion, selectivity as well as the reaction rate are listed accordingly.

$$N_{i_{inlet}}, N_{i_{outlet}} = \textit{mole flow rate of inlet or outlet component } i$$

$$C_{i_{inlet}}, C_{i_{outlet}} = \textit{mol \% of inlet or outlet component } i$$

$$Conversion, X\ (\%) = \frac{N_{ethane_{inlet}} - N_{ethane_{oulet}}}{N_{ethane_{inlet}}} \times 100\%$$

$$= \frac{C_{ethane_{inlet}} - C_{ethane_{oulet}}}{C_{ethane_{inlet}}} \times 100\%$$

$$Selectivity, S_{ethene}\ (\%) = \frac{N_{ethene_{outlet}}}{N_{ethane_{inlet}} - N_{ethane_{oulet}}} \times 100\%$$

$$= \frac{C_{ethene_{outlet}}}{C_{ethane_{inlet}} - C_{ethane_{oulet}}} \times 100\%$$

$$Rate, -r_{ethane}\ (mmol\ h^{-1} g_{cat}^{-1}) = \frac{X\ (\%) \times\ C_{ethane_{inlet}}(\%) \times SV(\frac{L}{g_{cat} \times h})}{24.5\ \times\ 10^{-3}\ (\frac{L}{mmol})}$$

The constant, 24.5 (L/mol), is the volume of one mole ideal gas at room temperature and 1 atm. The gases are assumed to be ideal gas for the convenience of calculation.

Chapter 3

NON-OXIDATIVE ETHANE DEHYDROGENATION

3.1 Catalysts Reactivity

In this section we are going to evaluate the effects of Ga atom in the mixed oxides in non-oxidative ethane dehydrogenation by measuring the reactivity of a series of Ga/Al_2O_3 catalysts. Figure 3 showed the effect of the surface composition of the different catalysts prepared on their activity by the plot of the reaction rate of ethane consumption in the packed bed reactor against time-on-stream.

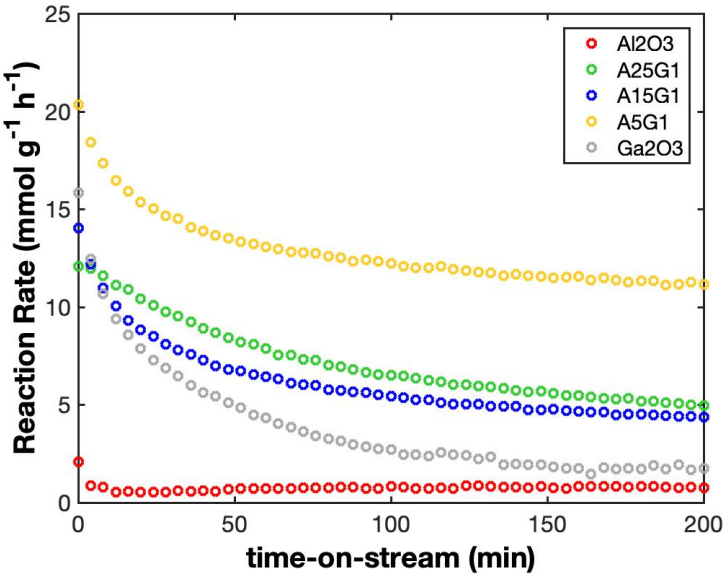

Figure 3: The catalyst performance of mixed oxide Ga_2O_3-Al_2O_3

Given the data, it can be calculated that he initial reaction rate of γ-Al_2O_3 is 2.09 ($mmol \cdot h^{-1} \cdot g_{cat}^{-1}$) and deactivated to 0.73 ($mmol \cdot h^{-1} \cdot g_{cat}^{-1}$) after 3 hr reaction, while the initial rate of Ga_2O_3 is 15.8 ($mmol \cdot h^{-1} \cdot g_{cat}$) and deactivated to 1.73 ($mmol \cdot h^{-1} \cdot g_{cat}^{-1}$) after 3 hr reaction. Initial rates and 3-hr rates of the above and other catalysts are shown

in Figure 4. The rates after 3 hr is 35%, 43%, 32%, 53% and 10.9% of the initial rate for AL, A25G1, A15G1, A5G1 and GA respectively.

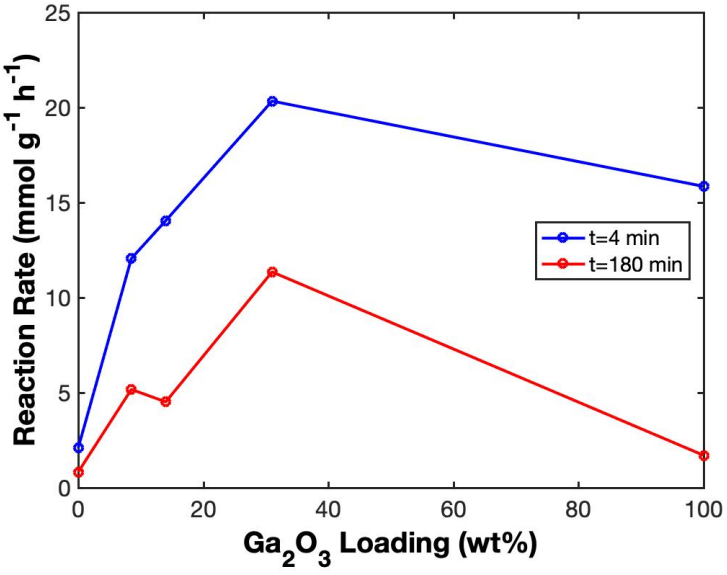

Figure 4: The effect of Ga_2O_3 content on the initial rate and the rate after 3 hours of EDH. The reaction (EDH) takes place at 3.6 kPa C_2H_6 in He at 600℃.

Addition of gallium increases the initial rate and a maximum is reached when the ratio of alumina to gallium is 5 to 1. The deactivation of mixed oxide is stronger of than that of pure alumina, but milder than that of pure gallia. Nevertheless, the activity of the A5G1 after 3 hr of reaction still remains at least 5 folds higher than that of either aluminum or gallium oxide.

To summarize, the synergetic effects of the mixed oxide have been identified significant on both activity as well as stability, and we would like to understand the role of Ga and Al respectively via further kinetic studies of the catalysts.

3.2 Kinetic Experiments

A series of kinetic studies were conducted over our Ga/Al_2O_3 catalysts as well as pure Al_2O_3 and Ga_2O_3. Kinetic parameters were obtained assuming a power law rate form as expressed in the following equation.

$$-r_{C_2H_6} = kP_{C_2H_6}^{\gamma}$$

$$k = k_0 e^{-\frac{E_a}{RT}}$$

Figure 5 and Figure 6 are illustrative figures from which we can obtain the kinetic parameters using A5G1 as the catalyst. With the measured reaction rate at different partial pressures as well as different temperatures, the reaction order was obtained in the log-log plot of reaction rate against partial pressure of ethane and the apparent activation energy was obtained using an Arrhenius plot. The rest of parameters for each catalyst can be found in Table 1, and the figures are in Appendix A.

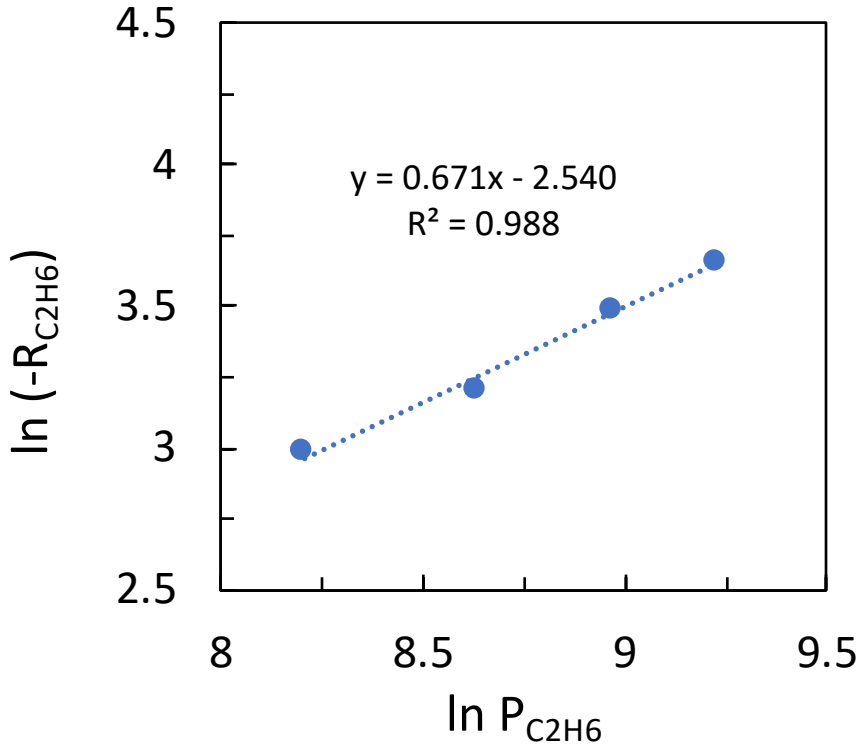

Figure 5: Log-Log plot of rate versus partial pressure of C_2H_6 to obtain reaction order of A5G1.

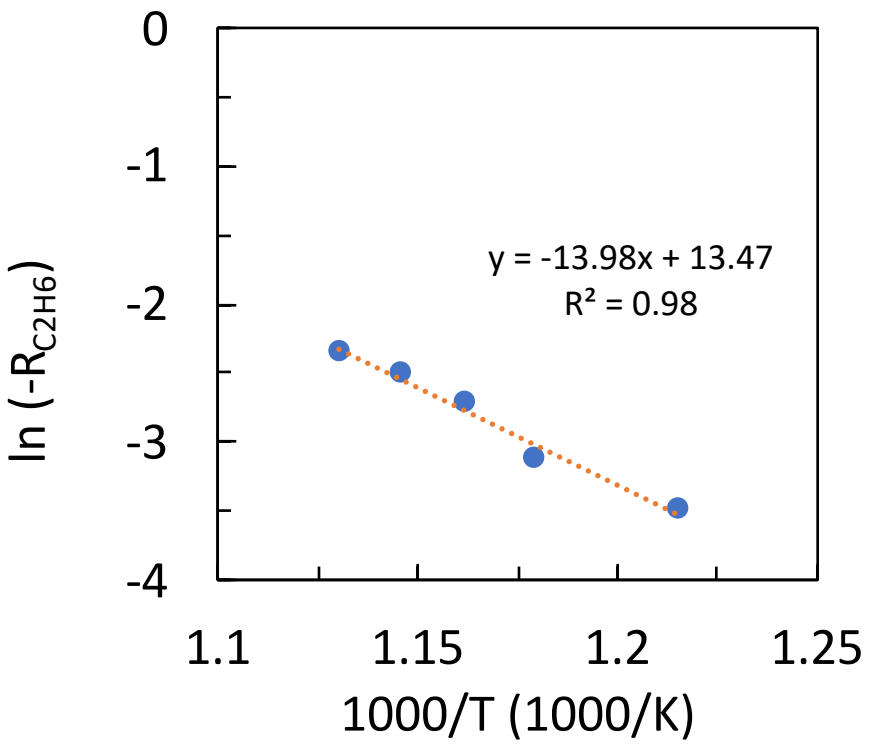

Figure 6: Arrhenius plot of rate versus 1000/Temperature to obtain activation energy of A5G1

Table 1: The Kinetic Parameters of Ga_2O_3-Al_2O_3 catalysts for EDH obtained by EDH

	Ea (kJ/mol)	Rate* (mmol/h/g_{cat})	ln k_0	Reaction Order on P_{C2H6}
Al_2O_3	191	1.53	18.64	1.14
A15G1	107	2.42	7.20	1.05
A5G1	119	19.83	13.47	0.67
Ga_2O_3	N/A	N/A	N/A	0.7

The ethane dehydrogenation can be described by two reaction mechanisms. The first is through the direct ethylene and hydrogen formation.[34] The other is the stepwise pathway through ethylene formation followed by the release of adsorbed hydrogen. The stepwise pathway requires two metal adsorption sites to proceed. The second metal site on the surface is then needed for the abstraction of the hydrogen.

Kinetic model based on Langmuir-Hinshelwood principles were derived to help us understand the kinetic parameters. For the ethane dehydrogenation, the reaction can be described by the following steps including the ethane adsorption, surface reaction, and the hydrogen desorption. For the ethane dehydrogenation, the rate determining is usually found to be either the first hydrogen abstraction (R4) or the second hydrogen abstraction (R5). Therefore, in the following part, we are going to derive the reaction rate law considering R4 or R5 as the rate determining step respectively.

$$C_2H_6 + * \overset{k_a, k_{-a}}{\longleftrightarrow} C_2H_6 * \quad \text{(R3)}$$

$$C_2H_6 * + * \overset{k_{s_1}, k_{-s_1}}{\longleftrightarrow} C_2H_5 * + H * \quad \text{(R4)}$$

$$C_2H_5 * \overset{k_{s_2}, k_{-s_2}}{\longleftrightarrow} C_2H_4 + H * \quad \text{(R5)}$$

$$2H * \overset{k_d, k_{-d}}{\longleftrightarrow} H_2 + 2 * \quad \text{(R6)}$$

We first consider the first hydrogen abstraction as the rate determining step and the rest are therefore in equilibrium. Based on these assumptions the reaction rate law will be expressed as described by the following expression:

$$r = \frac{k_{s_1} K_a P_{C_2H_6}}{\left[1 + K_a P_{C_2H_6} + \left(K_{s_2} P_{C_2H_4} + 1\right)\sqrt{K_d P_{H_2}}\right]^2}$$

The apparent reaction order on ethane will be between -1 to 1.

On the other hand, if we consider the second hydrogen abstraction as the rate determining step, the reaction other than second hydrogen abstraction were considered at equilibrium. As a result, the reaction rate law is described by the following equation:

$$r = \frac{k_s K_a P_{C_2H_6}}{K_{S_1}\sqrt{K_d P_{H_2}} + K_{S_1} K_d P_{H_2} + K_a\sqrt{K_d P_{H_2}} + K_a P_{C_2H_6}}$$

As can be seen, when the adsorption to ethane is weak, the reaction order on ethane will also approach to 1. The apparent reaction order on ethane will be between 0 to 1.

For AL and A15G1, the reaction order on ethane were observed as 1 while for GA and A5G1, the reaction order on ethane were found to be around 0.7 for AL and A15G1. According to the rate law predicted in previous section, we can infer that the adsorption of ethane is relatively unimportant with low surface concentration of gallium. The

reaction order decreases as gallium is added to the system indicating adsorption of ethane is more favorable on gallium.

The apparent activation energy using the pure alumina was 191 kJ/mol while it was 107 kJ/mol and 119 kJ/mol respectively for A15G1 and A5G1. This indicated that the addition of Ga atom reduces the energy barrier of using Al_2O_3 for ethane dehydrogenation.

In a collaborative work,[34] the molecular model of γ-Al_2O_3 as well as Ga/Al_2O_3 has been constructed based on density functional theory. The model was then used to build a microkinetic model for estimation of the kinetic parameters. In their calculations the reaction order of ethane was also found to be 1 for γ-Al_2O_3 and alumina with the surface modeled specified by one gallium per unit cell. On the other hand, the reaction order will be reduced to 0.7 for the model of two adjacent gallium per unit cell. The trend of experimental results is found to be consistent with computational method. The loading of Ga was low and there are more Ga_{III}-Al_{IV} sites and Al_{III}-Al_{IV} sites. On the other hand, for Ga_2O_3 and A5G1, there is higher amount of Ga, so more Ga_{III}-Ga_{IV} active sites could be found on the surface.

According to the DFT studies on the clean surface of Al_2O_3, the apparent activation energy is 49 kJ/mol, which is much lower than the experimental result. It is possible that the surface of the catalyst is partially hydro-oxylated, and that the clean surface was used in the computational model is not realistic. Additional work is required to reconcile experimental results with computation model.

Chapter 4

OXIDATIVE ETHANE DEHYDROGENATION

4.1 Catalyst Reactivity

In Figure 7, the observed reaction rate of each catalyst is plotted against on stream time for the oxidative ethane dehydrogenation using CO_2 (CO2EDH) as mild oxidant. The initial rates and final rates were compared in Figure 8. As in the case of EDH, the synergetic effects of the mixed oxide again out from the perspectives of both activity and stability. Pure alumina has poor catalytic activity to CO2EDH with its initial rate at 0.49 ($mmol \cdot h^{-1} \cdot g_{cat}^{-1}$) and rate after 3 hr at 0.22 ($mmol \cdot h^{-1} \cdot g_{cat}^{-1}$), 45% of the initial rate. On the other hand, pure gallia has high activity but poor stability. The initial rate using gallia was 20.7 ($mmol \cdot h^{-1} \cdot g_{cat}^{-1}$) and the rate after 3 hr reaction was 3.04 ($mmol \cdot h^{-1} \cdot g_{cat}^{-1}$), which is only 15% of the initial rate. Combining both advantages, the activity of mixed oxide could reach as high as that of the pure gallia, while the activity remains higher than 78% of the initial rate after 3 hr of reaction.

To specifically evaluate the effect of CO_2 in ethane dehydrogenation, we plot the time-on-stream conversion of both oxidative and non-oxidative reaction for each catalyst. Figure 9 showed the results of A5G1 on the left and A15G1 on the right. The addition of CO_2 enhanced the stability of the catalyst and promoted its activity in CO2 EDH. It should be noted that with A5G1, the initial rate of CO2EDH is already comparable to that of EDH using A5G1. The stability of the catalyst is much better than EDH. However, the stability of A5G1 is still inferior to A15G1 indicating that here is trade of between adding more gallium and stability.

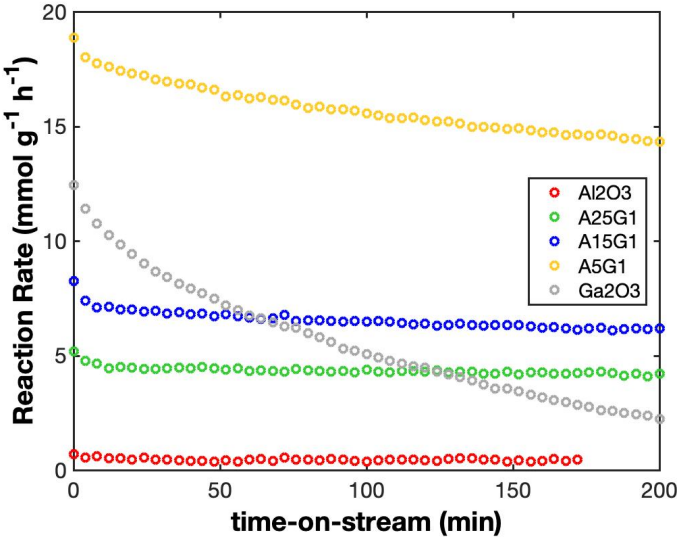

Figure 7: The catalyst performance of alumina, various mixed oxide Ga2O3-Al2O3 and gallium oxide in CO2ODH

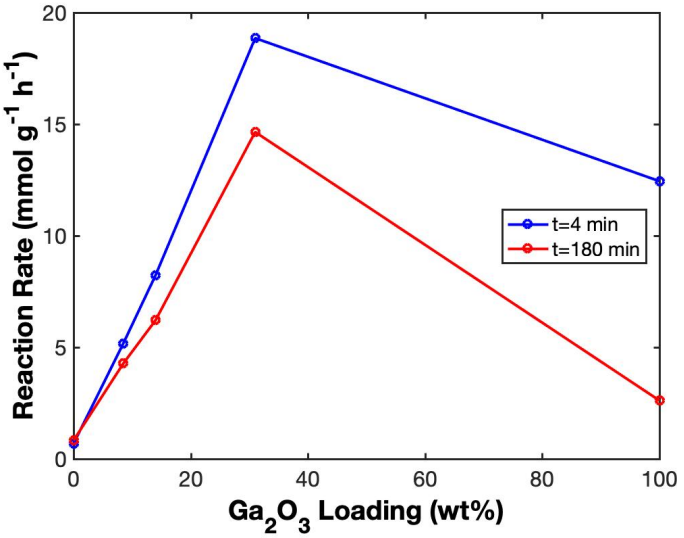

Figure 8: The effect of Ga_2O_3 content at the initial rate and the rate after 3 hr CO2EDH. The reaction (CO2EDH) was taking place at 3.6 kPa C_2H_6 + 3.6 kPa CO_2 in He at 600°C.

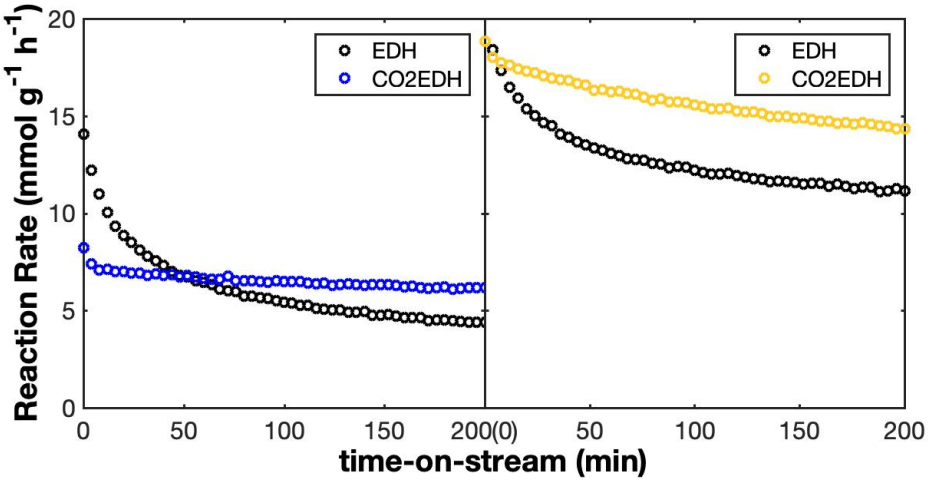

Figure 9: The effect of CO_2 in the ethane dehydrogenation using A15G1 (left) and A5G1 (right). The reaction was taking place at 1) 3.6 kPa C_2H_6 in He and 2) 3.6 kPa C_2H_6 + 3.6 kPa CO_2 in He at 600°C for EDH and CO2EDH separately.

4.2 Kinetics Experiments

For the investigation of kinetic parameters of initial oxidative ethane dehydrogenation, we added an equimolar CO_2 to C_2H_6 ratio into the gas feed. The reactions involved are in listed below. The direct ethane dehydrogenation (R7) is accompanied by the reverse water gas shift reaction (R8). Carbon dioxide will also react with the coke precursor to produce carbon monoxide through the reverse Boudouard reaction (R9). There is also a direct oxidative ethane dehydrogenation pathway (R10).

$$C_2H_6 \rightarrow C_2H_4 + H_2 \qquad \text{(R7)}$$

$$CO_2 + H_2 \rightarrow CO + H_2O \quad \text{(R8)}$$

$$CO_2 + C \rightarrow 2CO \quad \text{(R9)}$$

$$C_2H_6 + CO_2 \rightarrow C_2H_4 + CO + H_2O \quad \text{(R10)}$$

The function of CO_2 is to push the equilibrium forward through reverse water gas shift and to remove the coke from the surface of the catalyst increasing catalysts the stability. The power law expression of the reaction rate will become in the following form.

$$-r_{C_2H_6} = kP_{C_2H_6}^{\alpha} P_{CO_2}^{\boldsymbol{\beta}}$$

Figure 10 to Figure 12 are examples for the plots to obtain activation energy and reaction order for CO2EDH using A5G1. The plots for other catalysts are given in Appendix B, and all kinetic parameters are listed in Table 2.

It is observed that the reaction order on ethane, for oxidative dehydrogenation, is the same as that observed in the non-oxidative dehydrogenation. On the other hand, the reaction order on CO_2 is close to 0 regardless the Ga loading. The apparent activation energy was increased by the addition of CO_2 but showed the same trend with addition of Ga in EDH. Therefore, we expect that carbon dioxide is not directly involved in the dehydrogenation process.

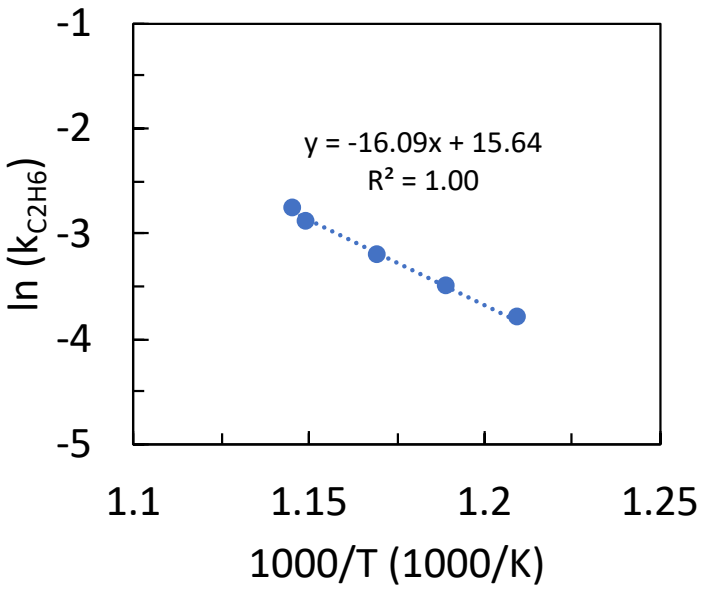

Figure 10: Arrhenius plot of A5G1 in CO2 EDH

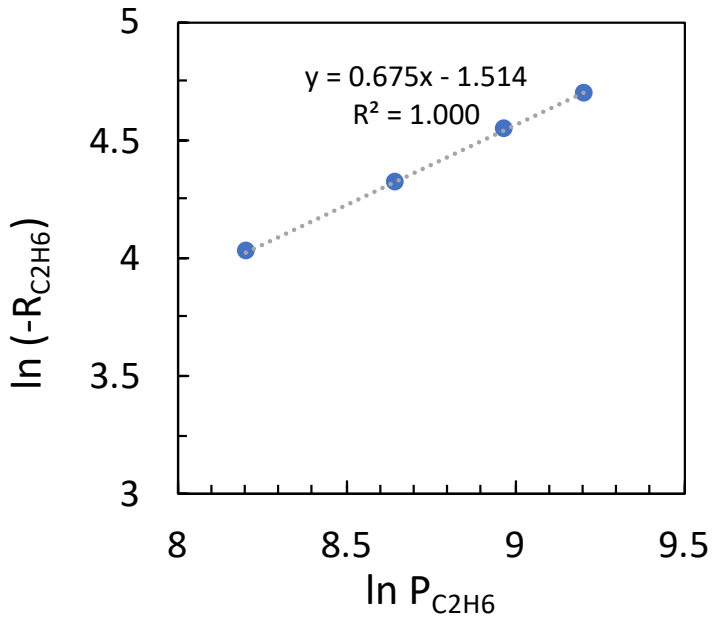

Figure 11: Log-Log plot of rate versus partial pressure of C_2H_6 to obtain reaction order of A5G1.

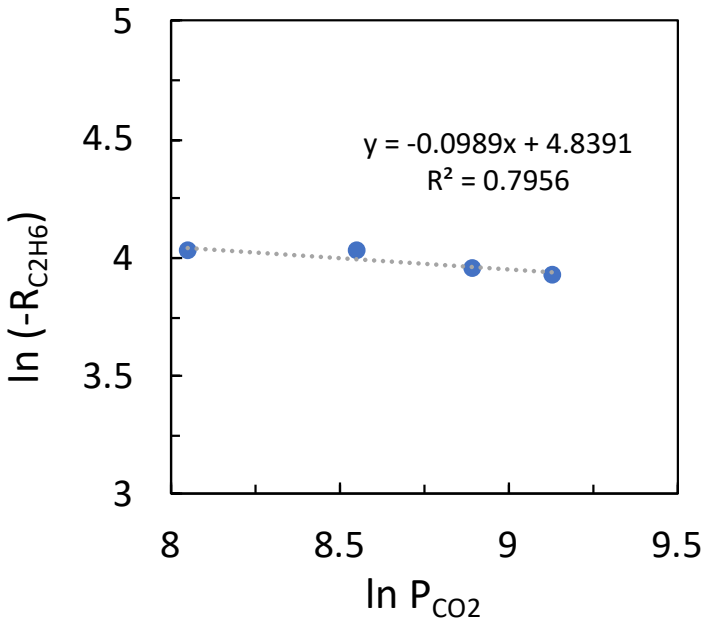

Figure 12: Log-Log plot of rate versus partial pressure of CO_2 to obtain reaction order of A5G1.

Table 2: CO2EDH kinetic Parameters of various Ga_2O_3-Al_2O_3 catalysts for CO2EDH.

	Ea (kJ/mol)	Rate* (mmol/h/g_{cat})	ln k_0	Reaction order on P_{C2H6}	Reaction order on P_{CO2}
Al_2O_3	253	0.48	25.30	1.04	-0.16
A15G1	119	8.61	8.81	1.16	0.11
A5G1	134	18.57	15.64	0.68	-0.10
Ga_2O_3	133	20.65	14.65	0.78	0.01

4.3 Deactivation Comparison Between EDH and CO2EDH

Although CO_2 does not directly participate into the reaction, there are other prominent ways that CO_2 can affect the reaction. Carbon dioxide has great influence on the rate of deactivation since it can react with coke through reverse Boudouard reaction.

The deactivation behavior can be expressed as an activity function in the following form:

$$a(t) = \frac{-r_{C_2H_4}(t)}{-r_{C_2H_4}(t=0)} \times 100\%$$

The activity function is plotted against the time-on-stream. The results of A15G1 are shown in Figure 13.

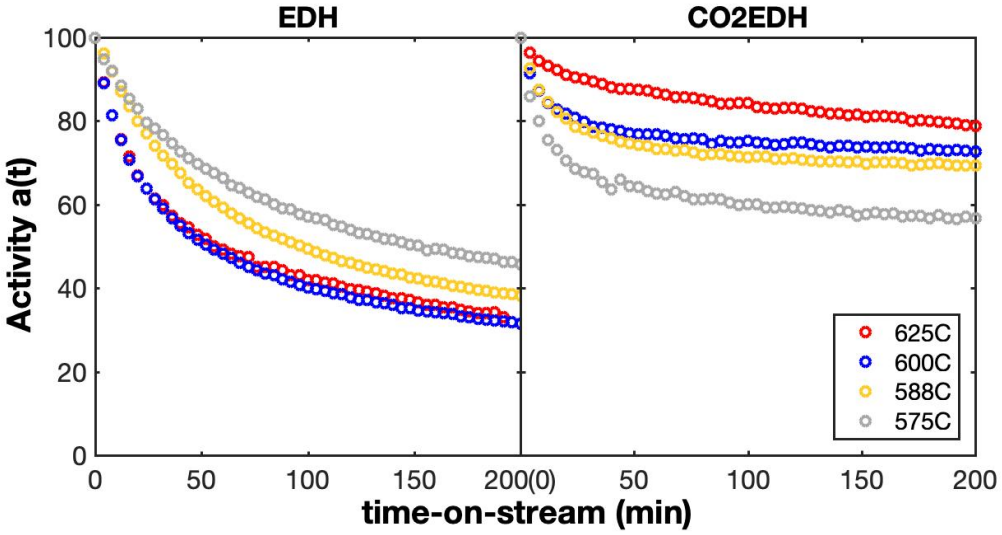

Figure 13: Deactivation behavior of the catalyst (A15G1) a) in the absence and b) in the presence of CO_2.

It was found that the temperature effects on deactivation of EDH and CO2EDH are completely different. Cracking reactions have higher endothermicity and their rates increase must faster with temperature. The left of Figure 13 showed that the deactivation increases with increasing temperature from 575ºC to 600 ºC. The deactivation at 625 ºC is comparable to that of 600ºC but slightly less. Higher temperature leads to higher cracking rates, higher coking and faster deactivation. However, a limit or maximum deactivation is found because initial coking will reduce adsorption and slower cracking. On the other hand, the deactivation rate for CO2EDH displayed an opposite trend. The deactivation rate is lower at higher temperature (Figure 13 right). The reaction rate after 3 hr reaction dropped to 50 % of the initial reaction rate at 588℃ while it dropped to about 30% of the initial rate at 625℃. The reverse Boudouard reaction is a highly

endothermic reaction which intakes 171 kJ/mol for the heat of the reaction. Therefore, we infer that main role of CO_2 is to removing surface carbon by the reverse Boudouard reaction in CO2EDH.

Chapter 5

CATALYST CHARACTERIZATION

5.1 BET measurements

Table 3: Surface area of catalysts

	γ-Al_2O_3	A15G1	A5G1	Ga_2O_3
Specific surface area (m^2/g)	120	245	200	34.5

The γ-Al_2O_3 itself is a type of porous materials while Ga_2O_3 has low specific surface area. On the other hand, it is shown that the specific surface area of mixed oxides is higher than that for both pure alumina and gallia in Table 3. The co-precipitation method can provide a route to synthesize material with higher surface area. The high surface area with well distributed active sites is one of the main reasons that the co-precipitation method is frequently used in the preparation for catalysts.

5.2 XRD

The XRD patterns of prepared Ga/Al_2O_3 indicate that the crystal structure of the catalysts is γ-Al_2O3 like (Figure 14). No crystal structure of Ga_2O_3 was found. Their broader peak width indicates the grain size may be smaller and the crystal structure is less perfect mixed oxides. The lattice parameter (a_0) of the cubic lattice of γ-alumina can be estimated based on the d_{440} spacings. A proportional relationship was also identified between the lattice parameter and the Ga content as indicated in Figure 15. The decreasing d_{440} spacing with increasing Ga composition in the co-precipitation procedure is an evidence of Ga atom was cooperated into the bulk of Al_2O_3 without the formation Ga oxide crystal.[44] The higher the Ga composition in the co-precipitation

procedure more Ga are doped into the bulk of γ-Al_2O_3, leading to greater unit cell dimensions.

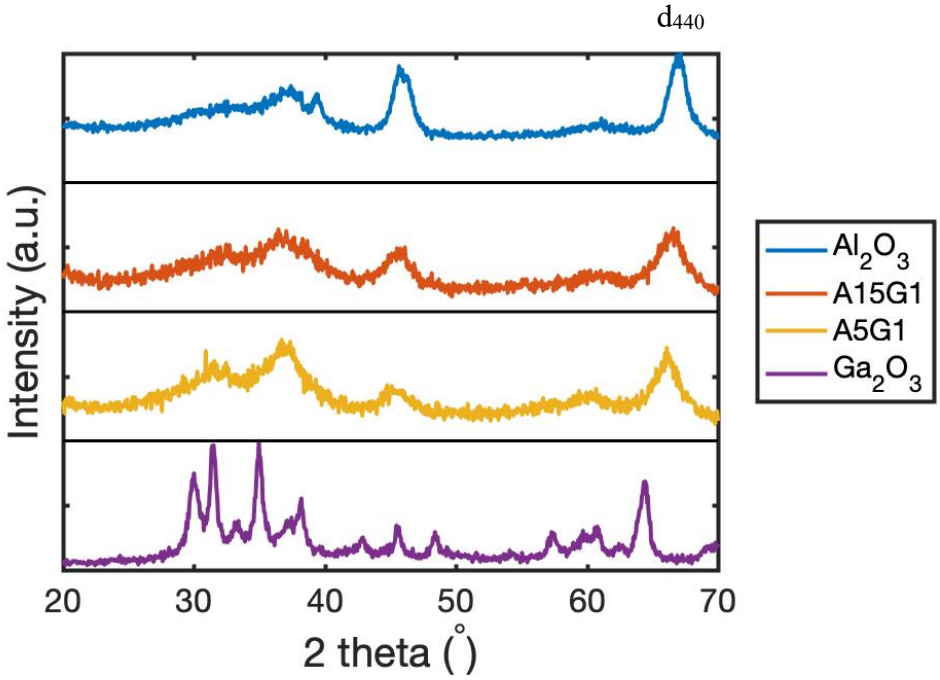

Figure 14: XRD patterns of Ga/Al_2O_3 catalysts.

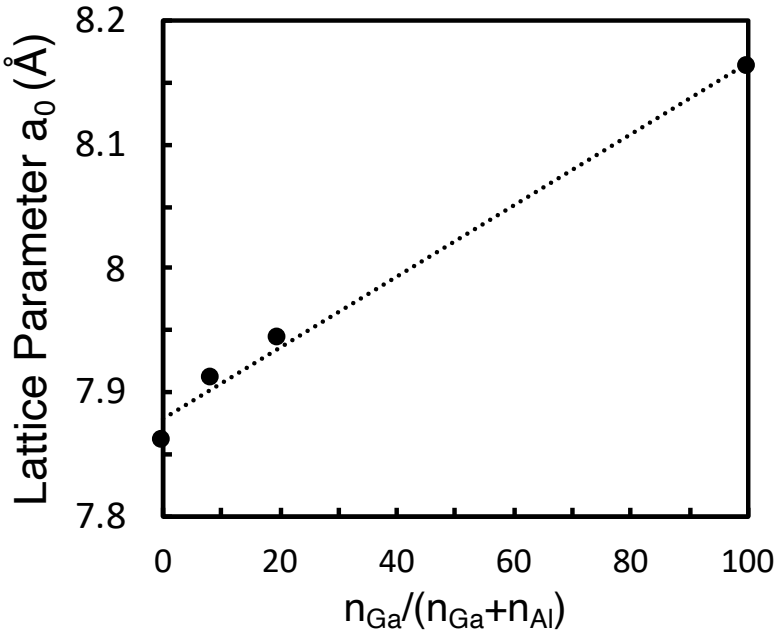

Figure 15: Lattice parameter a_0 versus Ga content.

5.3 MAS Nuclear Magnetic Resonance (NMR) Spectroscopy

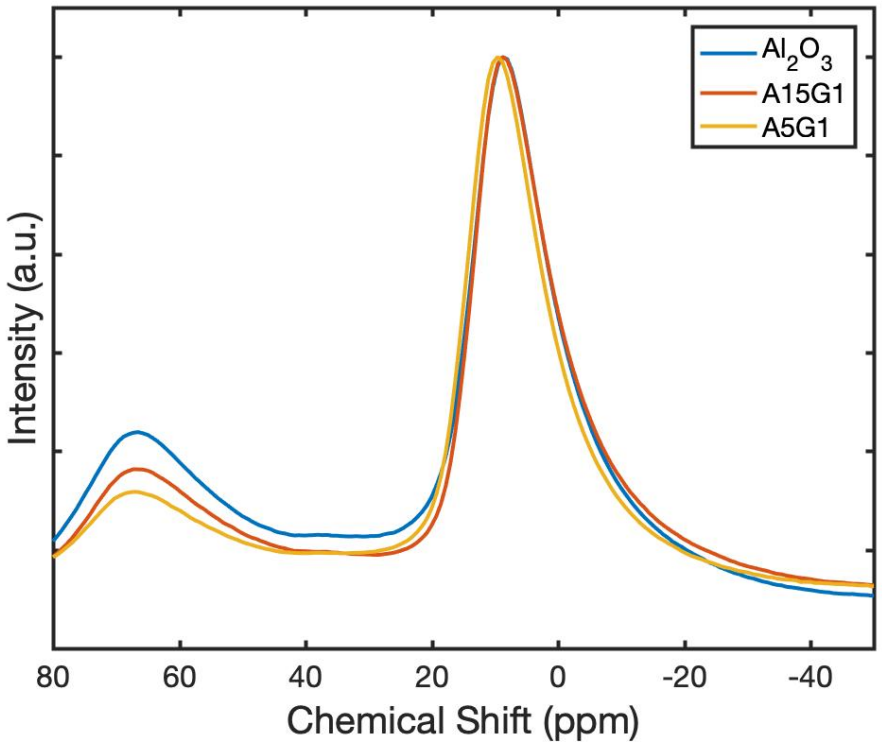

Figure 16: ^{27}Al MAS NMR spectra of different catalysts

Magic angle spinning (MAS) NMR spectroscopy is frequently used to understand the coordination on Al atoms in a metal oxide.[44]–[46] ^{27}Al chemical shift is sensitive to the number of coordination site and geometry of the aluminum atom. The shape of coordination sites is a factor that can affect chemical shift and peak shape and width, but generally, the number of neighboring atoms is the dominant effect. In an γ-Al_2O_3 model, we expect there are Al_{IV}, Al_V and Al_{VI} on the catalysts. The peak position of Al_{IV}, Al_V and Al_{VI} are located at 68 ppm, 34 ppm and 10 ppm, respectively, in the NMR

spectrum. In the ^{27}Al MAS NMR spectrum displayed in Figure 16 and Figure 17, a decreasing Al_{IV}/Al_{VI} is observed as the Ga content increases. This is an indicator that the Ga atoms are incorporated into the bulk of Al_2O_3 and occupied the tetrahedral Al sites. However, the Al_V site is not observed in this case indicating a neglectable number of Al_V site existing in the catalyst.

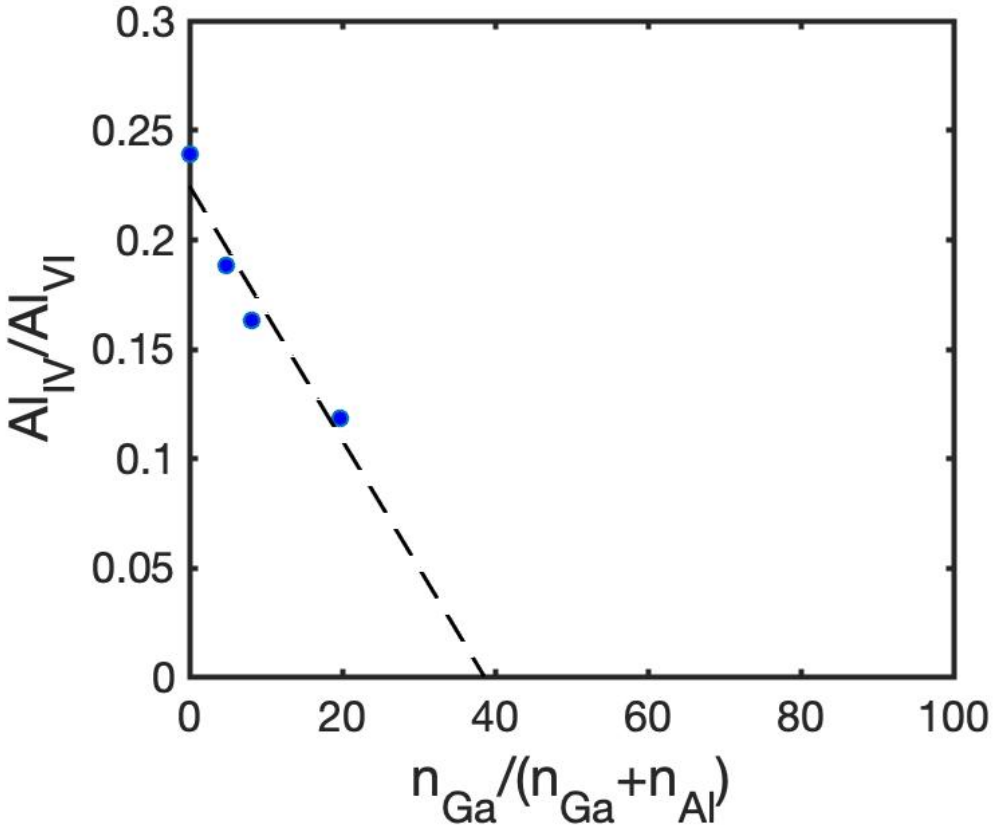

Figure 17: The ratio of Al_{IV} to Al_{VI} against the loading of Ga.

5.4 X-ray Photoelectronic Spectrometry (XPS)

In the survey scan from XPS of each catalyst (Table 4), we can find there is only very slight increase in binding energy of Al 2p. There is almost no change in binding

energy for Ga 3/2p as Ga is added to the catalyst. Although Ga elements were found incorporated into the Al bulk by observing the XRD pattern, it does not change the oxidation state of Al atom. Vice versa, the Ga atom pertain the same oxidation environment as Ga^{3+} in mixed gallium aluminum oxide as it does in the pure Ga_2O_3.[47]

From the XPS results, we can also obtain the surface Ga/Al atomic ratio. If the gallium and aluminum oxide were precipitate out uniformly during the precipitation process, the surface Ga to Al ratio should equal to the ration in the bulk. The ratio is decided by the ratio in the mixed nitrate precursor, and it is 6.7% and 20% respectively for A15G1 and A5G1. However, the surface Ga to Al ratio is in fact much lower than the predicted ratio. This indicated that most of the gallium atoms are incorporated into the bulk of the alumina. The surface Ga to Al ratio on the surface is 3% and 9% respectively for A15G1 and A5G1. In the computational surface model according to our collaborator, it is 10% and 20% of Ga to Al ratio for the case of single Ga atom per unit cell and the case of two Ga atom per unit cell respectively.[34]

Table 4: XPS results for catalysts.

Name of Catalysts	Al_2O_3	A15G1	A5G1	Ga_2O_3
Al atomic %	43.5	38.2	34.9	0.0
Ga atomic %	0.0	1.3	3.3	20.3
C atomic %	8.3	11.0	14.0	23.4
O atomic %	48.2	49.6	50.9	56.4
Al 2p BE (eV)	74.24	74.65	74.89	N/A
Ga 3/2p BE (eV)	N/A	1118.58	1119.11	1119.00
surface Ga/Al atomic ratio	0.00	0.03	0.09	inf

Table 5: Results of XPS before and after ethane dehydrogenation using A15G1

	0 hr EDH	6 hr EDH	30 hr EDH	6hr CO2EDH	30 hr CO2EDH
Al 2p BE (eV)	74.80	74.57	74.76	74.65	74.55
Ga 3/2p BE (eV)	1118.97	1118.47	1118.59	1118.66	1118.49
Al 2p FWHM (eV)	2.24	1.63	1.58	1.95	1.60
Ga 3/2 p FWHM (eV)	2.78	2.03	2.09	2.34	2.07

Table 5 presented the peak position and width of Al 2p and Ga 3/2p scan after the dehydrogenation and regeneration in both oxidative and non-oxidative cases. There is no obvious shift in binding energy after reaction and regeneration for both Al 2p and Ga 3/2p. However, both peaks were also found sharpen after reaction, probably due to heat treatment in the regeneration procedure.

Chapter 6

COKE CHARACTERIZATION

The amount and the structure of the coke forming on the catalyst are also important pieces of information that help evaluate the effect of CO_2 in ethane dehydrogenation process. Therefore, TGA, XPS, and TEM were used to obtain the information of coke.

6.1 Thermogravimetric Analysis (TGA)

To measure the amount of coke formation, TGA was utilized to quantify the amount of coke in air as a function of temperature (Figure 18). For the spent catalysts used in EDH, the amount of coke was approximately 5.2% and 6.5% w/w of the spent catalyst after 6 hr and 30 hr reaction respectively. For the spent catalysts used in CO2EDH, the amount of coke was only about 2.2% and 6.0%. The discrepancy of the amount of coke between 6 hr EDH and 6 hr CO2EDH clearly indicates the ability of CO_2 for decreasing coke formation. On the other hand, the ability of CO_2 in decreasing coke diminished at longer reaction times. The analysis of TGA traces can be used to complement the XPS spectra discussed in the next section.

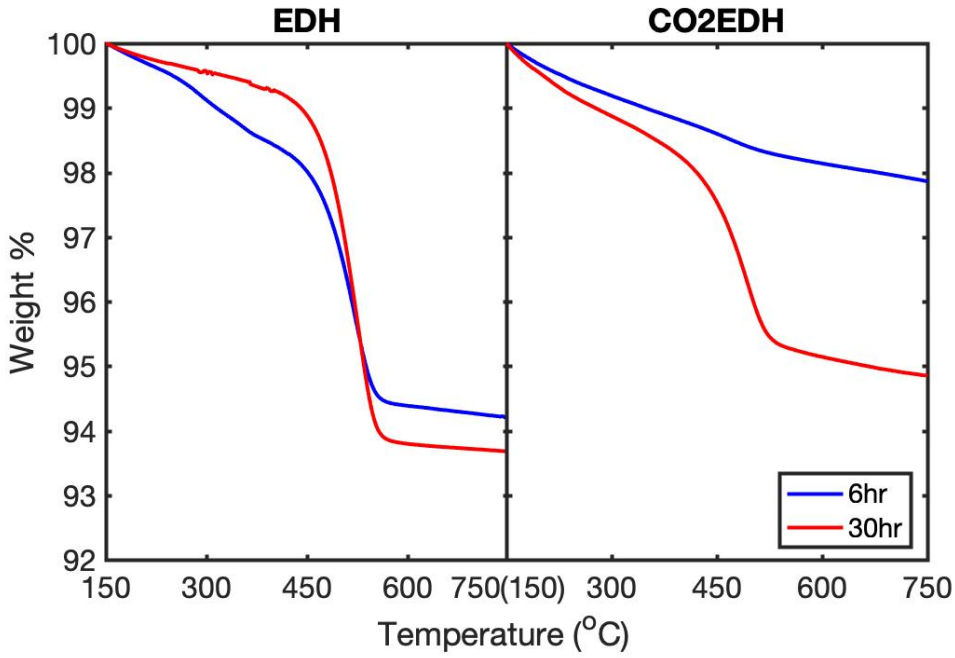

Figure 18: The weight % loss against temperature for the spent catalysts after 6 hours and 30 hours of EDH and CO2EDH.

6.2 Transmission Electronic Microscopy (TEM)

Different types of coke can be deposited on the catalyst during EDH. Under TEM (Figure 19 left), a layer-by-layer structure was clearly observed on the surface of the spent catalyst (6 hr of EDH using Al5G1). Its structure and length of d-spacing help us identify it as graphitic coke.[48] On the other hand, the amorphous coke was found non-uniformly distributed on the catalyst, randomly forming clusters (Figure 19 right).

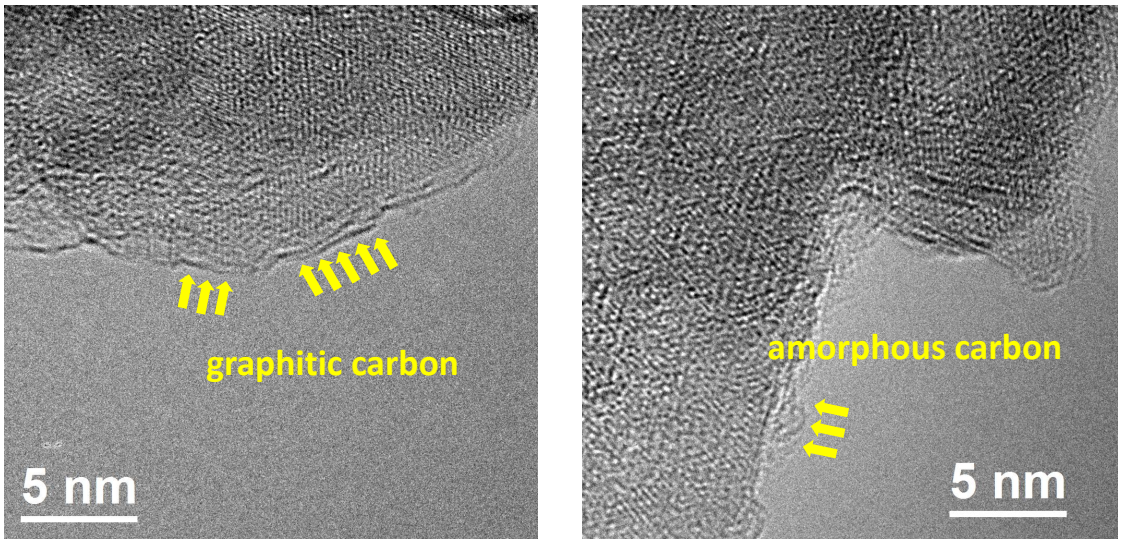

Figure 19: Left: Graphitic coke and RightL amorphous coke on the surface of catalyst (6hr EDH).

6.3 X-ray Photoelectronic Spectrometry (XPS)

Since different types of coke were formed, we can use XPS to evaluate the coke structure on the surface of the spent catalysts. The C1s scan provides the information about the surface carbon structure, which was mainly contributed by the building of coke after deactivation. While the graphitic coke only contributes to sp2 carbon, the amorphous coke contributes to both sp3 and sp2 carbon. Therefore, XPS spectra can shed light by semi-quantitatively identifying the structural evolution of coke on the surface of the catalyst.

In Figure 20 (a), the deconvolution of C1s scan is displayed. The deconvolution of C1s was based on previous report.[49] Please see Appendix for each C1s deconvolution

spectra of A15G1. On the fresh catalyst, the sp3 carbon signal was due to adventitious carbon, which can be found for all materials which was stored in air.[49]–[51] Therefore, the peak position of sp3 carbon (284.8 eV) is usually utilized as a calibration reference of peak position. In Figure 20 (b), we can find that the sp2 carbon quickly build up after 6 hr deactivation from EDH, while there is no sp2 carbon found in CO2EDH for the same reaction time. On the other hand, we can visually identify the coke built up for both cases because the white catalyst turns black. Therefore, it is expected that only amorphous coke built-up after 6 hr CO2EDH while both amorphous coke and graphitic coke were both formed after 6 hr EDH. When we extended the reaction time to 30 hr, only sp2 carbon was found on the surface regardless the addition of CO_2, implying that the graphitic structure could be the final destination of the coke evolution.

Combining TGA and XPS results, we can infer that CO_2 only efficiently suppress coke formation at the stage where coke is mostly amorphous. However, when coke becomes graphitic, CO_2 does not affect the formation rates of coke any longer.

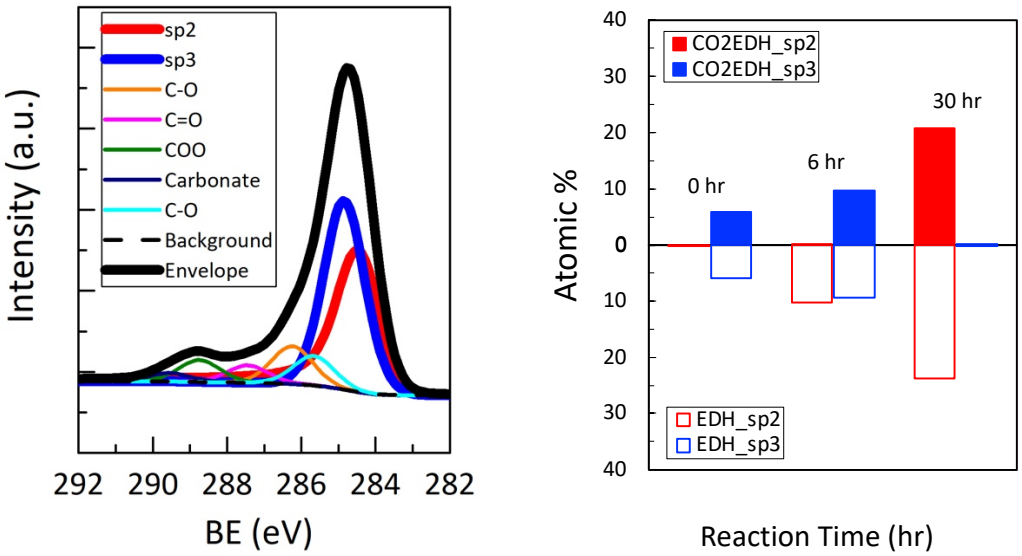

(a) (b)

Figure 20: a) The C1s deconvolution spectrum in XPS for A15G1 after 6 hr EDH b) The atomic % of carbon element on the surface of the catalyst (A15G1) after 0, 6 hr and 30 hr deactivation.

Chapter 7

CONCLUSION

In this work, an optimized composition of Ga_2O_3-Al_2O_3 synthesized via co-precipitation method is identified for the ethane dehydrogenation considering both catalytic reactivity and stability. The reactivity of mixed oxide can reach as high as that of Ga_2O_3 when the surface Ga/Al atomic ratio reaches around 0.1. The stability of the mixed oxide is also much improved compared with that of the pure Ga_2O_3.

The kinetic parameters were collected for Ga_2O_3-Al_2O_3 with different composition of Ga. It is found the that the reaction order on ethane is a dependent parameter of the amount of Ga in the mixed oxide for both non-oxidative and oxidative ethane dehydrogenation. The reaction order is close to 1 when the surface Ga/Al ratio is below 0.1 while it is close to 0.7 for the higher composition of Ga. We can infer from the dependency that there is a transfer of the active sites on the surface of the catalyst from Al sites to Ga sites as the increasing Ga loading. The activation energy decreases when the Ga is added on the surface of the catalyst. It shows that Ga sites on the surface provide a route with a lower energy barrier for the cleavage of the C-H bond of ethane. The addition of CO_2, on the other hand, has no effect on the activation energy and the reaction order. The reaction order on CO_2 is close to zero for all catalysts. Therefore, we conclude that CO_2 does not direct participate in the rate determining step of the reaction.

Then the effect of CO_2 is observed from the perspective of catalytic stability. In non-oxidative ethane dehydrogenation, the side cracking reactions are more active as the temperature increased, and hence accelerate the deactivation. However, the opposite

deactivation behavior is observed in the oxidative ethane dehydrogenation using A15G1 catalyst. CO_2 has the ability to oxidize the carbonaceous components accumulated on the surface of the catalyst from the side cracking reactions, which is also a highly endothermic reaction. Therefore, the rate deactivation is reduced as the increasing temperature due to the faster removal of the coke precursors.

The effect of CO_2 on the removal of coke precursors was characterized. The amount of coke was reduced in the oxidative condition after 6 hr of the reaction. The structure of coke was also found to be amorphous at this point in the oxidative condition while it was partially graphitic in the non-oxidative condition. It indicates that CO_2 has the ability to prevent the accumulation and the propagation of coke from carbonaceous components to graphitic coke. However, the carbonaceous components will eventually propagate into graphitic structure despite of the presence of CO_2 given that the amount and the structure of coke became the same in both oxidative and non-oxidative condition for 30 hr.

In conclusion, we identified an optimized composition of Ga_2O_3-Al_2O_3 for ethane dehydrogenation. We also tempt to explain the relationship between active sites on the catalyst and the catalytic reactivity as well as the stability in terms of the kinetic parameters. CO_2 was also found to be a promising alternative to oxygen on the issue of extension of the catalyst lifetime in ethane dehydrogenation without the sacrifice of the selectivity to ethylene.

REFERENCES

[1] B. Wire, “United States Ethylene Market Analysis & Outlook 2019-2023 - ResearchAndMarkets.com.” [Online]. Available: https://oglinks.news/exxonmobil/pr/united-states-ethylene-market-analysis-outlook-2019-2023-researchandmarkets.

[2] Icis, “Ethylene Uses and Market Data.” [Online]. Available: https://www.icis.com/explore/resources/news/2007/11/05/9075777/ethylene-uses-and-market-data.

[3] F. Cavani, N. Ballarini, and A. Cericola, “Oxidative dehydrogenation of ethane and propane: How far from commercial implementation?,” *Catal. Today*, vol. 127, no. 1–4, pp. 113–131, 2007.

[4] J. A. Labinger and J. E. Bercaw, “ChemInform Abstract: Understanding and Exploiting C-H Bond Activation,” *ChemInform*, vol. 33, no. 48, p. no-no, 2010.

[5] F. Kakiuchi and N. Chatani, “Catalytic Methods for C□H Bond Functionalization: Application in Organic Synthesis,” *Adv. Synth. Catal.*, vol. 345, no. 910, pp. 1077–1101, 2003.

[6] J. J. H. B. Sattler *et al.*, “Platinum-Promoted Ga/Al $_2$ O $_3$ as Highly Active, Selective, and Stable Catalyst for the Dehydrogenation of Propane,” *Angew. Chemie Int. Ed.*, vol. 53, no. 35, pp. 9251–9256, 2014.

[7] J. H. Sinfelt, “Hydrogenolysis of ethane over supported platinum,” *J. Phys. Chem.*, vol. 68, no. 2, pp. 344–346, 1964.

[8] R. D. Cortright, R. M. Watwe, and J. A. Dumesic, “Ethane hydrogenolysis over platinum selection and estimation of kinetic parameters,” *J. Mol. Catal. A Chem.*, vol. 163, no. 1–2, pp. 91–103, 2000.

[9] N. Rahimi and R. Karimzadeh, “Catalytic cracking of hydrocarbons over modified ZSM-5 zeolites to produce light olefins: A review,” *Appl. Catal. A Gen.*, vol. 398, no. 1–2, pp. 1–17, 2011.

[10] C. H. Bartholomew, “Mechanisms of catalyst deactivation,” *Appl. Catal. A Gen.*, vol. 212, no. 1–2, pp. 17–60, 2001.

[11] S. Tan *et al.*, “Propane Dehydrogenation over In2O3-Ga2O3-Al2O3Mixed Oxides,” *ChemCatChem*, vol. 8, no. 1, pp. 214–221, 2016.

[12] J. McGregor *et al.*, “Active coke: Carbonaceous materials as catalysts for alkane dehydrogenation,” *J. Catal.*, vol. 269, no. 2, pp. 329–339, 2010.

[13] M. D. Argyle and C. H. Bartholomew, “Heterogeneous catalyst deactivation and regeneration: A review,” *Catalysts*, vol. 5, no. 1, pp. 145–269, 2015.

[14] J. J. H. B. Sattler, J. Ruiz-Martinez, E. Santillan-Jimenez, and B. M. Weckhuysen, “Catalytic dehydrogenation of light alkanes on metals and metal oxides,” *Chem. Rev.*, vol. 114, no. 20, pp. 10613–10653, 2014.

[15] H. Z. Wang *et al.*, “Coke Formation on Pt-Sn/Al2O3 Catalyst for Propane Dehydrogenation,” *Ind. Eng. Chem. Res.*, vol. 57, no. 26, pp. 8647–8654, 2018.

[16] Q. Li, Z. Sui, X. Zhou, Y. Zhu, J. Zhou, and D. Chen, “Coke formation on Pt-Sn/Al2O3catalyst in propane dehydrogenation: Coke characterization and kinetic study,” *Top. Catal.*, vol. 54, no. 13–15, pp. 888–896, 2011.

[17] T. C. Da Silva, R. P. Dos Santos, N. Batalha, and M. M. Pereira, “Vanadium-potassium-alumina catalyst: A way of promoting CO2and coke reaction in the presence of O2during the FCC catalyst regeneration,” *Catal. Commun.*, vol. 51, pp. 42–45, 2014.

[18] M. Chen, J. Xu, Y. M. Liu, Y. Cao, H. Y. He, and J. H. Zhuang, “Supported indium oxide as novel efficient catalysts for dehydrogenation of propane with carbon dioxide,” *Appl. Catal. A Gen.*, vol. 377, no. 1–2, pp. 35–41, 2010.

[19] N. Y. Usachev *et al.*, “Oxidative conversion of ethane involving lattice oxygen of molybdenum systems modified with aluminum, gallium, or yttrium oxide,” *Pet. Chem.*, vol. 56, no. 9, pp. 841–845, 2016.

[20] S. Horikoshi, M. Kamata, T. Sumi, and N. Serpone, “Selective heating of Pd/AC catalyst in heterogeneous systems for the microwave-assisted continuous hydrogen evolution from organic hydrides: Temperature distribution in the fixed-bed reactor,” *Int. J. Hydrogen Energy*, vol. 41, no. 28, pp. 12029–12037, 2016.

[21] Z. Skoufa, E. Heracleous, and A. A. Lemonidou, “On ethane ODH mechanism and nature of active sites over NiO-based catalysts via isotopic labeling and methanol sorption studies,” *J. Catal.*, vol. 322, pp. 118–129, 2015.

[22] P. Michorczyk, “Dehydrogenation of propane to propene over gallium oxide in the presence of CO2,” *Appl. Catal. A Gen.*, vol. 251, no. 2, pp. 425–433, 2003.

[23] J. J. H. B. Sattler *et al.*, “Platinum-Promoted Ga/Al 2 O 3 as Highly Active, Selective, and Stable Catalyst for the Dehydrogenation of Propane,” *Angew. Chemie Int. Ed.*, vol. 53, no. 35, pp. 9251–9256, 2014.

[24] M. M. Bhasin, J. H. McCain, B. V. Vora, T. Imai, and P. R. Pujadó, “Dehydrogenation and oxydehydrogenation of paraffins to olefins,” *Appl. Catal. A Gen.*, vol. 221, no. 1–2, pp. 397–419, 2001.

[25] M. W. Schreiber *et al.*, “Lewis-Brønsted acid pairs in Ga / H-ZSM-5 to catalyze dehydrogenation of light alkanes Lewis-Brønsted acid pairs in Ga / H-ZSM-5 to catalyze dehydrogenation of light alkanes,” 2018.

[26] E. Heracleous and A. A. Lemonidou, “Reaction pathways of ethane oxidative and non-oxidative dehydrogenation on γ-Al2O3studied by temperature-programmed reaction (TP-reaction),” *Catal. Today*, vol. 112, no. 1–4, pp. 23–27, 2006.

[27] C. T. Shao, W. Z. Lang, X. Yan, and Y. J. Guo, “Catalytic performance of gallium oxide based-catalysts for the propane dehydrogenation reaction: effects of support and loading amount,” *RSC Adv.*, vol. 7, no. 8, pp. 4710–4723, 2017.

[28] Y. V. Joshi and K. T. Thomson, “The roles of gallium hydride and Brønsted acidity in light alkane dehydrogenation mechanisms using Ga-exchanged HZSM-5 catalysts: A DFT pathway analysis,” *Catal. Today*, vol. 105, no. 1 SPEC. ISS., pp. 106–121, 2005.

[29] M. W. Schreiber *et al.*, “Lewis-Brønsted Acid Pairs in Ga/H-ZSM-5 to Catalyze Dehydrogenation of Light Alkanes,” *J. Am. Chem. Soc.*, vol. 140, no. 14, pp. 4849–4859, 2018.

[30] A. Ausavasukhi and T. Sooknoi, “Tunable activity of [Ga]HZSM-5 with H2 treatment: Ethane dehydrogenation,” *Catal. Commun.*, vol. 45, pp. 63–68, 2014.

[31] B. Xu, T. Li, B. Zheng, W. Hua, Y. Yue, and Z. Gao, “Enhanced stability of HZSM-5 supported Ga2O3 catalyst in propane dehydrogenation by dealumination,” *Catal. Letters*, vol. 119, no. 3–4, pp. 283–288, 2007.

[32] T. Kiyoharu Nakagawa, Chiaki Kajita, Yuichiro IdeMasato, OkamuraShinjiro, KatoHitoshi Kasuya, Na-oki Ikenaga, Tetsuhiko Kobayashi and O. Suzuki, “Promoting effect of carbon dioxide on the dehydrogenation and aromatization of ethane over gallium-loaded catalysts,” *Catal. Letters*, vol. 64, no. 2–4, pp. 215–221, 2000.

[33] M. Chen *et al.*, “Dehydrogenation of propane over spinel-type gallia-alumina solid solution catalysts,” *J. Catal.*, vol. 256, no. 2, pp. 293–300, 2008.

[34] S. B. Praneet, “A DFT Calculation for the Mechanism studies of Ethane Dehydrogenation over Ga2O3/Al2O3.”

[35] F. Klose, M. Joshi, C. Hamel, and A. Seidel-Morgenstern, “Selective oxidation of ethane over a VO x /γ-Al 2 O 3 catalyst - Investigation of the reaction network,” *Appl. Catal. A Gen.*, vol. 260, no. 1, pp. 101–110, 2004.

[36] A. Farjoo, F. Khorasheh, S. Niknaddaf, and M. Soltani, “Kinetic modeling of side reactions in propane dehydrogenation over Pt-Sn/γ-Al2O3 catalyst,” *Sci. Iran.*, vol. 18, no. 3 C, pp. 458–464, 2011.

[37] F. Cavani and F. Trifirò, “The oxidative dehydrogenation of ethane and propane as an alternative way for the production of light olefins,” *Catal. Today*, vol. 24, no. 3, pp. 307–313, 1995.

[38] F. Cavani, N. Ballarini, and A. Cericola, “Oxidative dehydrogenation of ethane and propane: How far from commercial implementation?,” *Catal. Today*, vol. 127, no. 1–4, pp. 113–131, 2007.

[39] P. Michorczyk, K. Zeńczak, R. Niekurzak, and J. Ogonowski, “Dehydrogenation of propane with CO2 - A new green process for propene and synthesis gas production,” *Polish J. Chem. Technol.*, vol. 14, no. 4, pp. 77–82, 2012.

[40] M. A. Atanga, F. Rezaei, A. Jawad, M. Fitch, and A. A. Rownaghi, “Oxidative dehydrogenation of propane to propylene with carbon dioxide,” *Appl. Catal. B Environ.*, vol. 220, no. August 2017, pp. 429–445, 2018.

[41] K. Nakagawa, M. Okamura, N. Ikenaga, T. Suzuki, and T. Kobayashi, “Dehydrogenation of Ethane over Gallium Oxide in the Presence of Carbon Dioxide,” *Chem. Commun.*, vol. 3, no. 9, pp. 1025–1026, 1998.

[42] K. Nakagawa *et al.*, “Role of carbon dioxide in the dehydrogenation of ethane over gallium-loaded catalysts,” *J. Catal.*, vol. 203, no. 1, pp. 87–93, 2001.

[43] B. Xu, B. Zheng, W. Hua, Y. Yue, and Z. Gao, “Support effect in dehydrogenation of propane in the presence of CO2 over supported gallium oxide catalysts,” *J. Catal.*, vol. 239, no. 2, pp. 470–477, 2006.

[44] T. N. Afonasenko *et al.*, “Synthesis and properties of γ-Ga2O3–Al2O3 solid solutions,” *Russ. J. Phys. Chem. A*, vol. 91, no. 10, pp. 1939–1945, 2017.

[45] D. Lee, N. T. Duong, O. Lafon, and G. De Paëpe, “Primostrato solid-state NMR enhanced by dynamic nuclear polarization: Pentacoordinated Al3+ ions are only located at the surface of hydrated γ-alumina,” *J. Phys. Chem. C*, vol. 118, no. 43, pp. 25065–25076, 2014.

[46] T. H. Chen, B. H. Wouters, and P. J. Grobet, “Aluminium coordinations in zeolite mordenite by 27Al multiple quantum mas NMR spectroscopy,” *Eur. J. Inorg. Chem.*, no. 2, pp. 281–285, 2000.

[47] H. Chen, J. Hu, G. D. Li, Q. Gao, C. Wei, and X. Zou, “Porous Ga-In Bimetallic Oxide Nanofibers with Controllable Structures for Ultrasensitive and Selective Detection of Formaldehyde,” *ACS Appl. Mater. Interfaces*, vol. 9, no. 5, pp. 4692–4700, 2017.

[48] B. Kwiecińska and H. I. Petersen, “Graphite, semi-graphite, natural coke, and natural char classification-ICCP system,” *Int. J. Coal Geol.*, vol. 57, no. 2, pp. 99–116, 2004.

[49] S. Dutta *et al.*, “Solventless C-C Coupling of Low Carbon Furanics to High Carbon Fuel Precursors Using an Improved Graphene Oxide Carbocatalyst,” *ACS Catal.*, vol. 7, no. 6, pp. 3905–3915, 2017.

[50] K. Axis, “background and baseline in Peak Fitting in XPS,” pp. 1–29, 2006.

[51] P. Swift, “Adventitious carbon—the panacea for energy referencing?,” *Surf. Interface Anal.*, vol. 4, no. 2, pp. 47–51, 1982.

Appendix A

Log-Log Plots and Arrhenius Plots for Non-Oxidative Ethane Dehydrogenation of Each Catalysts

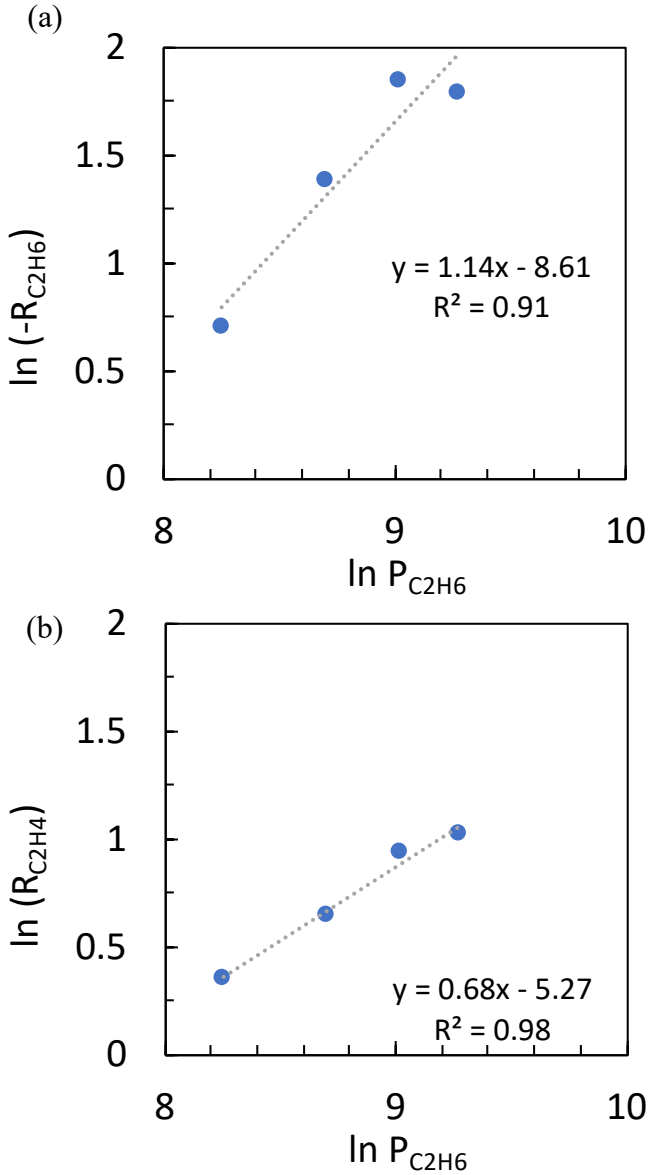

Figure A- 1: Log-Log plot of a) rate of C_2H_6 consumption and b) rate of C_2H_4 formation versus partial pressure of C_2H_6 to obtain reaction order using γ-Al_2O_3.

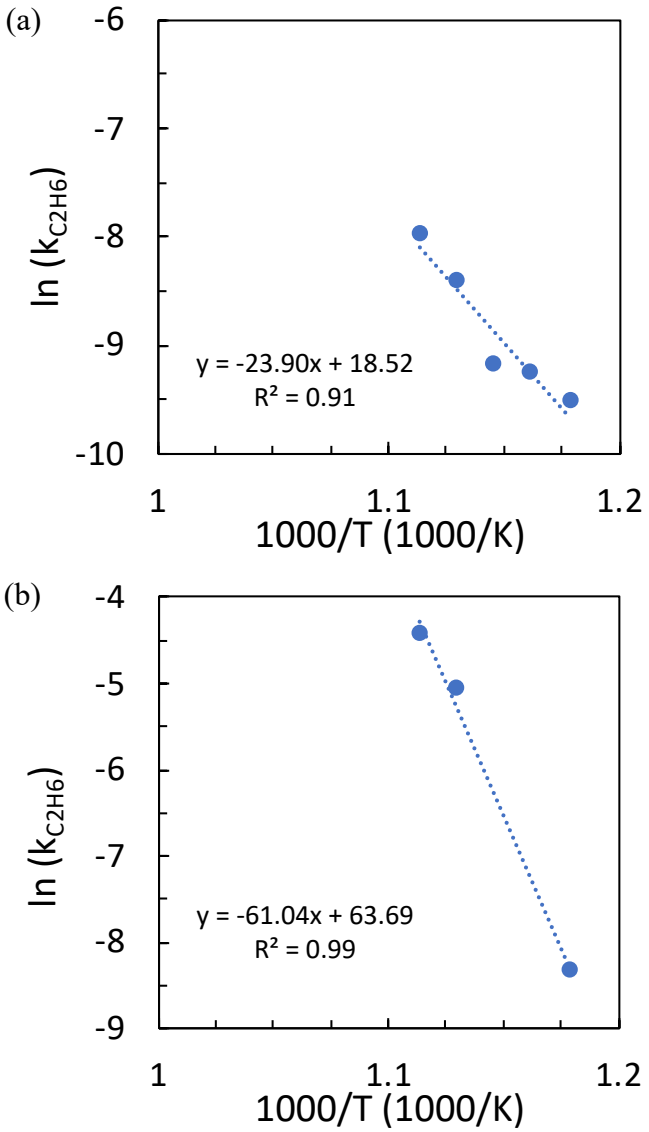

Figure A- 2: Arrhenius plot of a) C_2H_6 consumption and b) of C_2H_4 using γ-Al_2O_3.

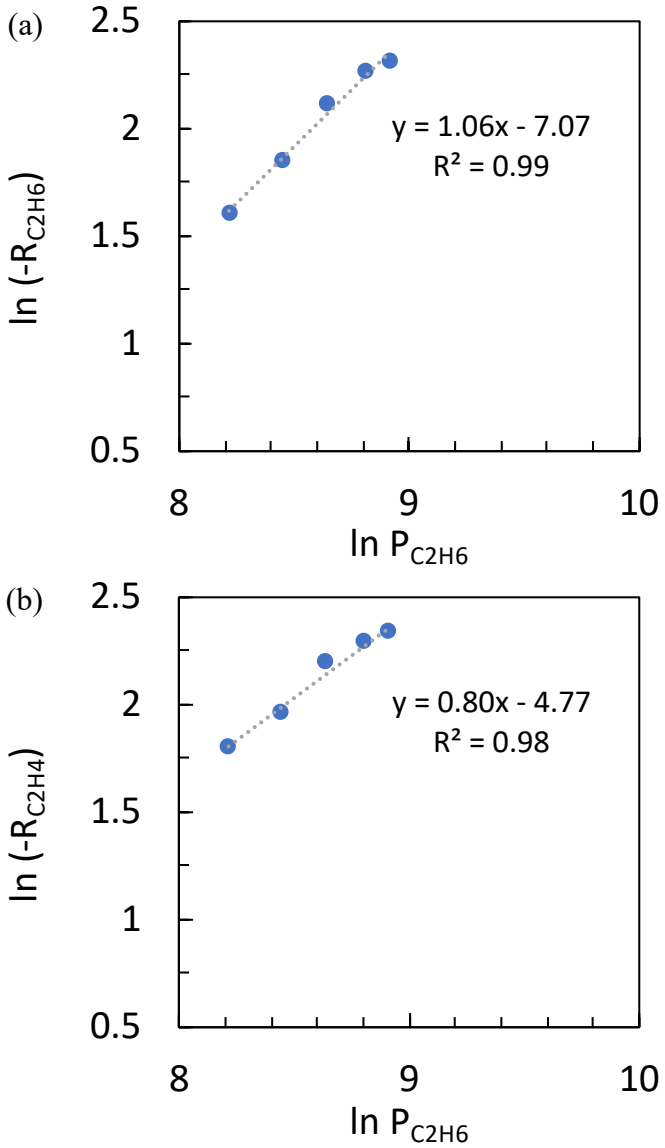

Figure A- 3: Log-Log plot of a) rate of C_2H_6 consumption and b) rate of C_2H_4 formation versus partial pressure of C_2H_6 to obtain reaction order using A15G1.

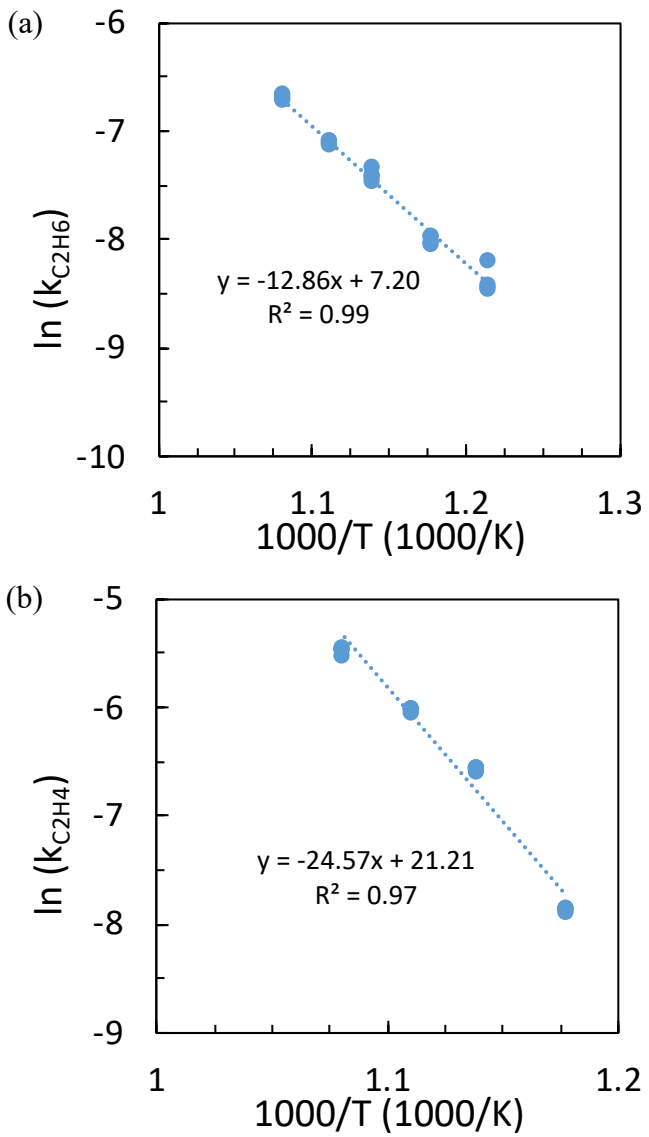

Figure A- 4: Arrhenius plot of a) C_2H_6 consumption and b) of C_2H_4 using A15G1.

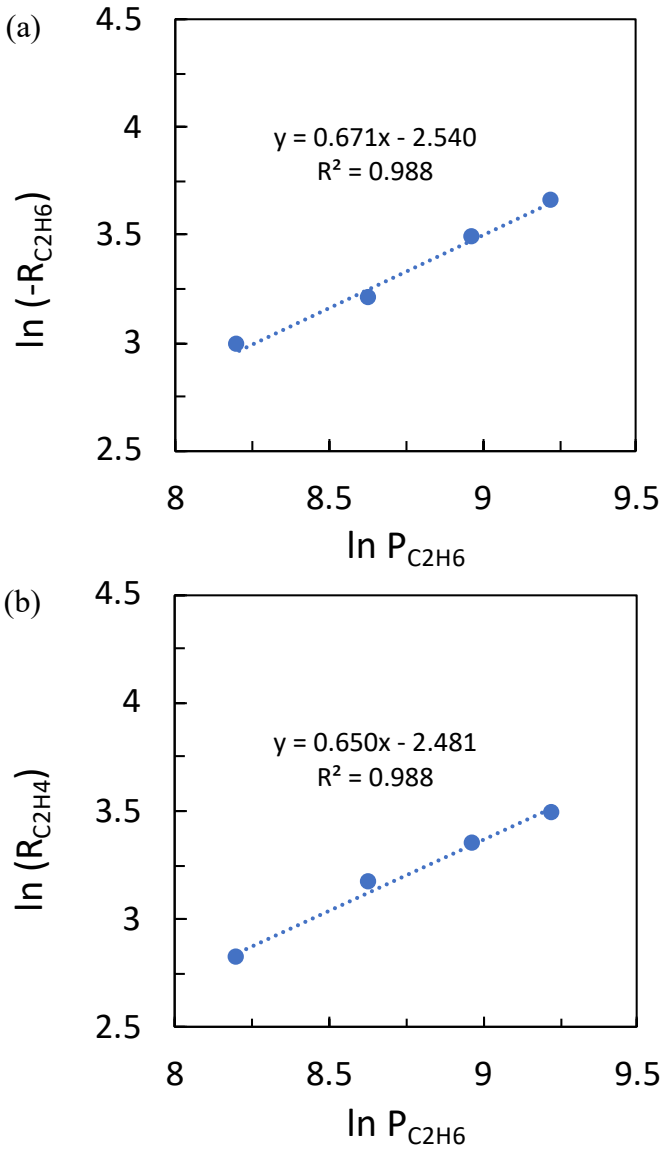

Figure A- 5: Log-Log plot of a) rate of C_2H_6 consumption and b) rate of C_2H_4 formation versus partial pressure of C_2H_6 to obtain reaction order using A5G1.

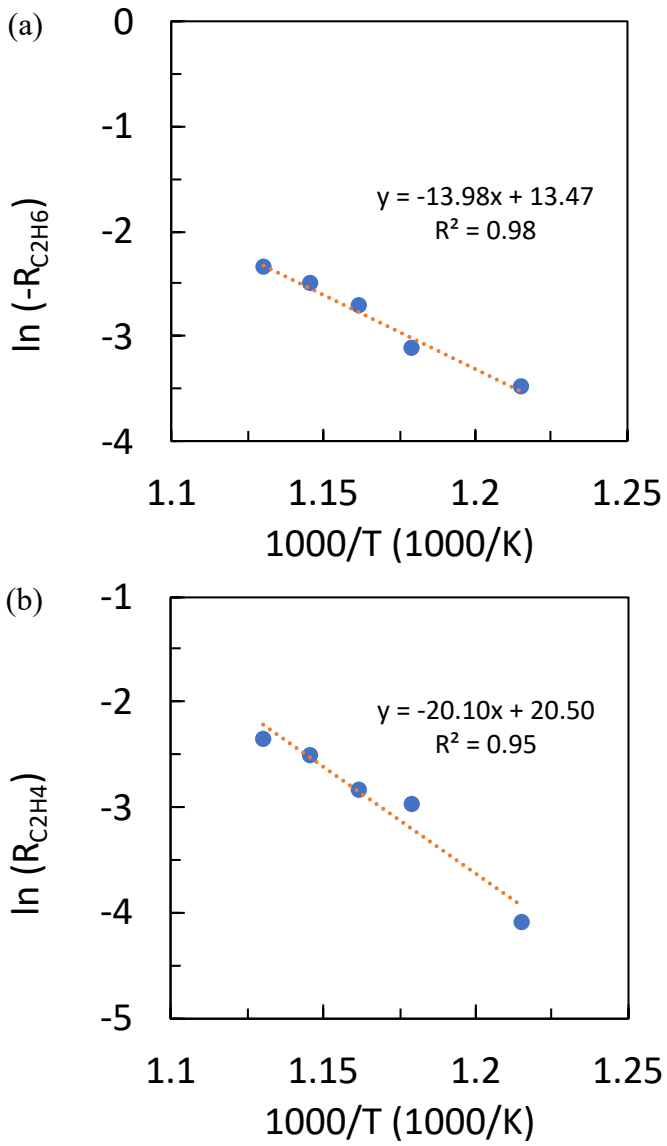

Figure A- 6: Arrhenius plot of a) C_2H_6 consumption and b) of C_2H_4 using A5G1.

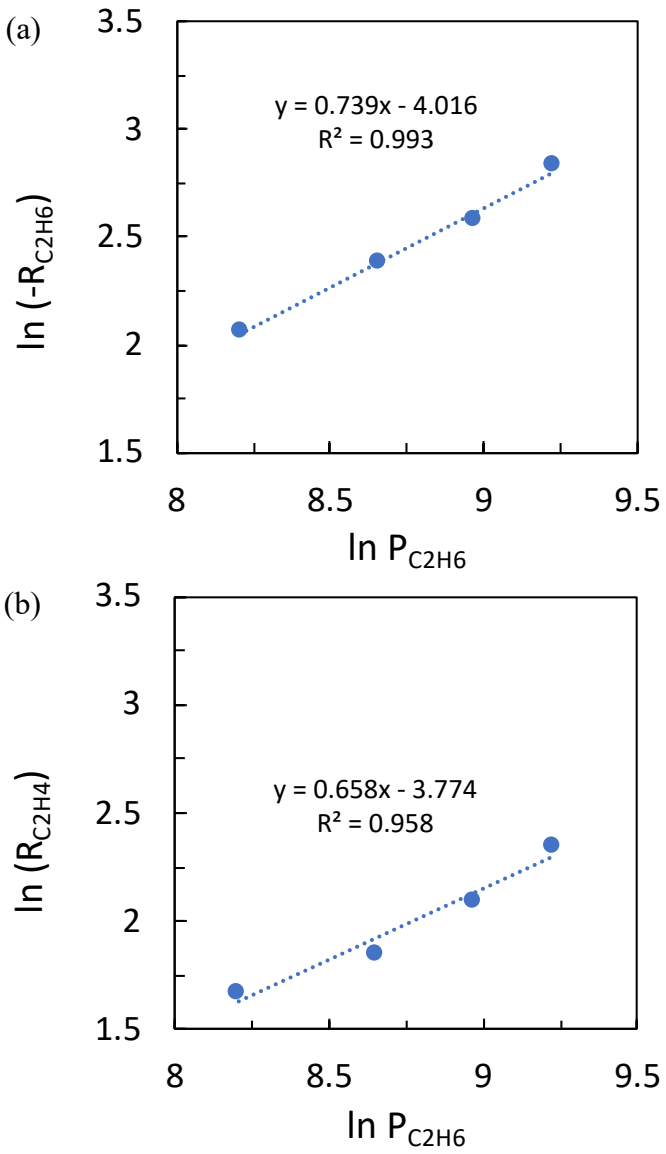

Figure A- 7: Log-Log plot of a) rate of C_2H_6 consumption and b) rate of C_2H_4 formation versus partial pressure of C_2H_6 to obtain reaction order using Ga_2O_3.

Appendix B

Log-Log Plots and Arrhenius Plots for Oxidative Ethane Dehydrogenation of Each Catalysts

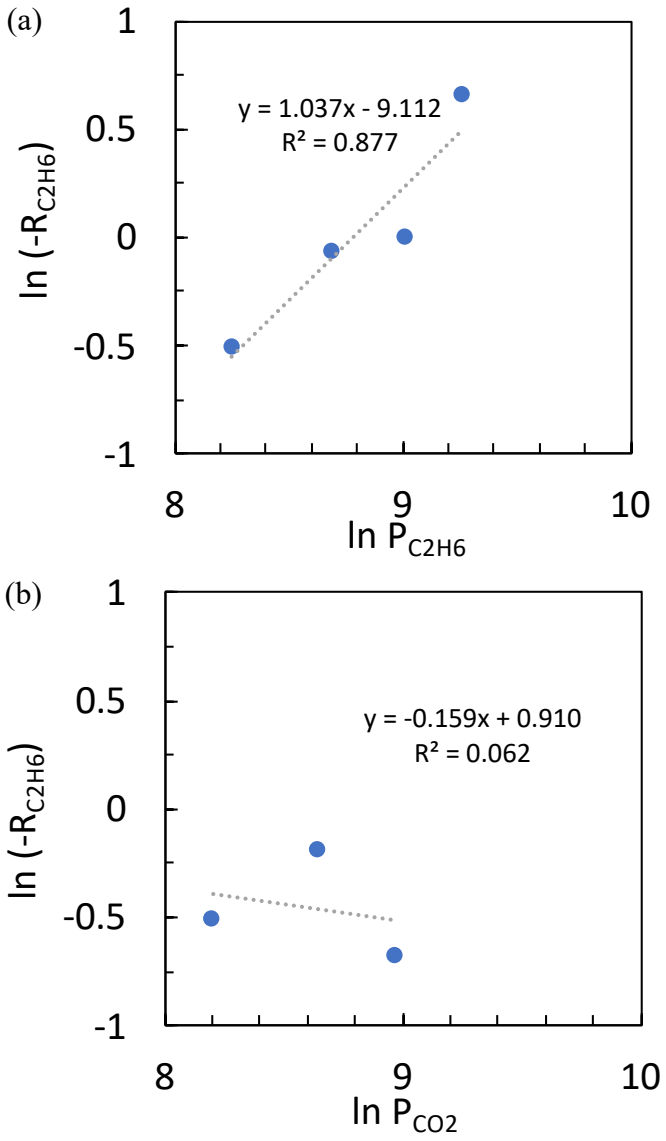

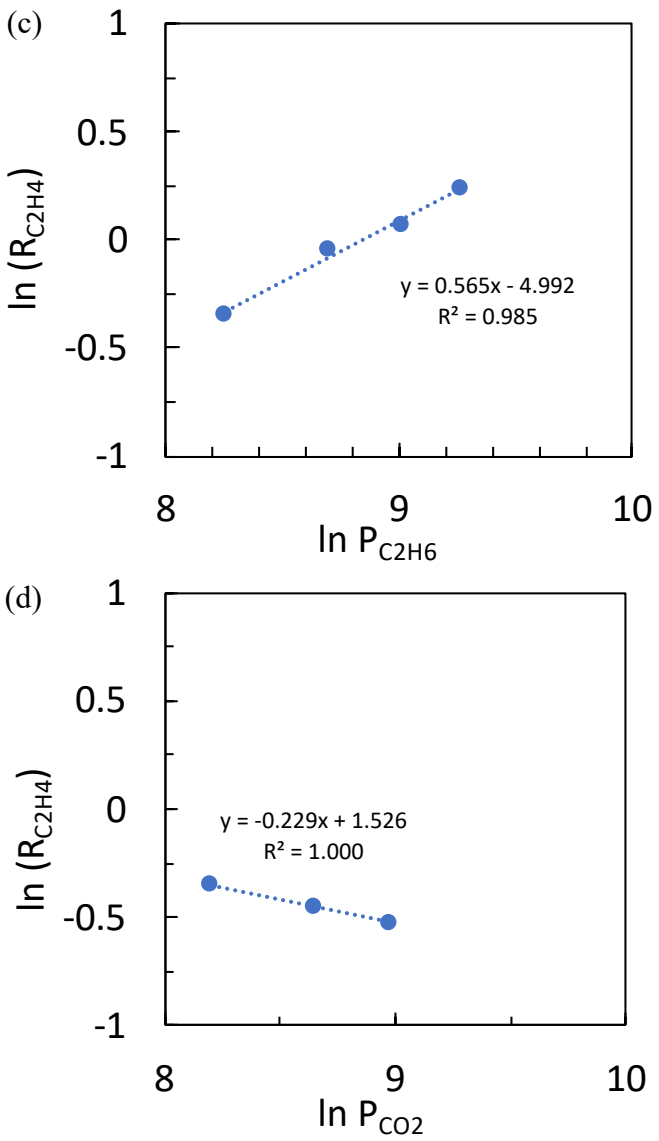

Figure B- 1: Log-Log plot of a) rate of C_2H_6 consumption, b) rate of C_2H_4 formation versus partial pressure of C_2H_6 and c) rate of C_2H_6 consumption, d) rate of C_2H_4 formation versus partial pressure of CO_2 to obtain reaction order using γ-Al_2O_3.

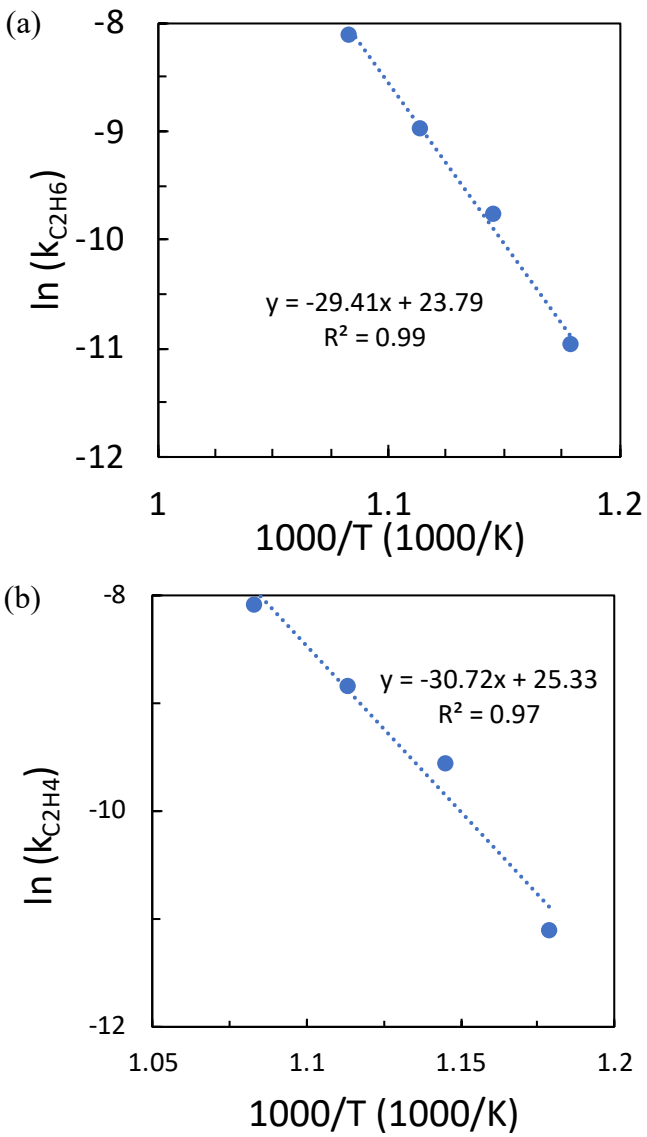

Figure B- 2: Arrhenius plot of a) C_2H_6 consumption and b) of C_2H_4 using γ-Al_2O_3.

(a)

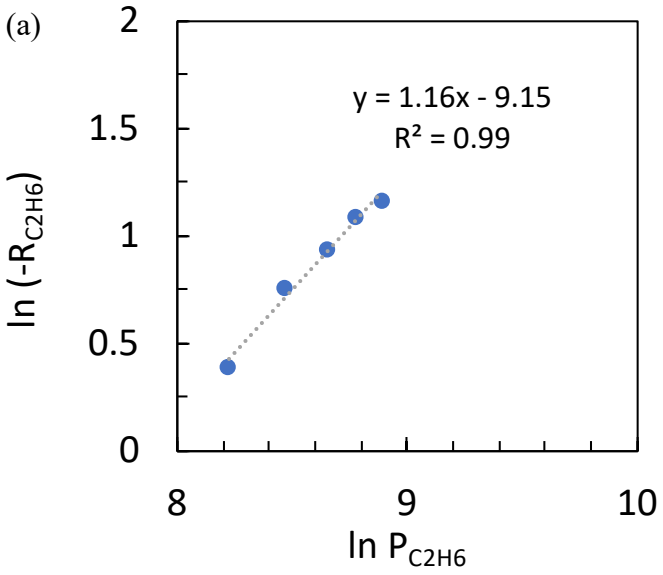
y = 1.16x - 9.15
R² = 0.99
ln (-R_C2H6)
ln P_C2H6
2
1.5
1
0.5
0
8
9
10

(b)

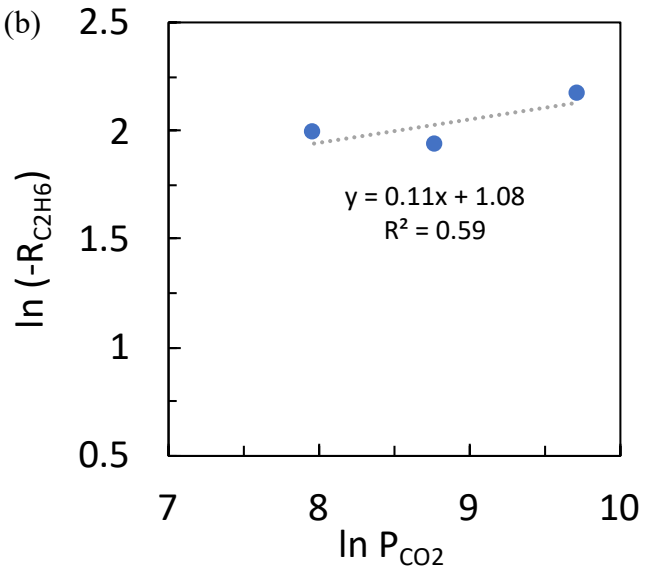
y = 0.11x + 1.08
R² = 0.59
ln (-R_C2H6)
ln P_CO2
2.5
2
1.5
1
0.5
7
8
9
10

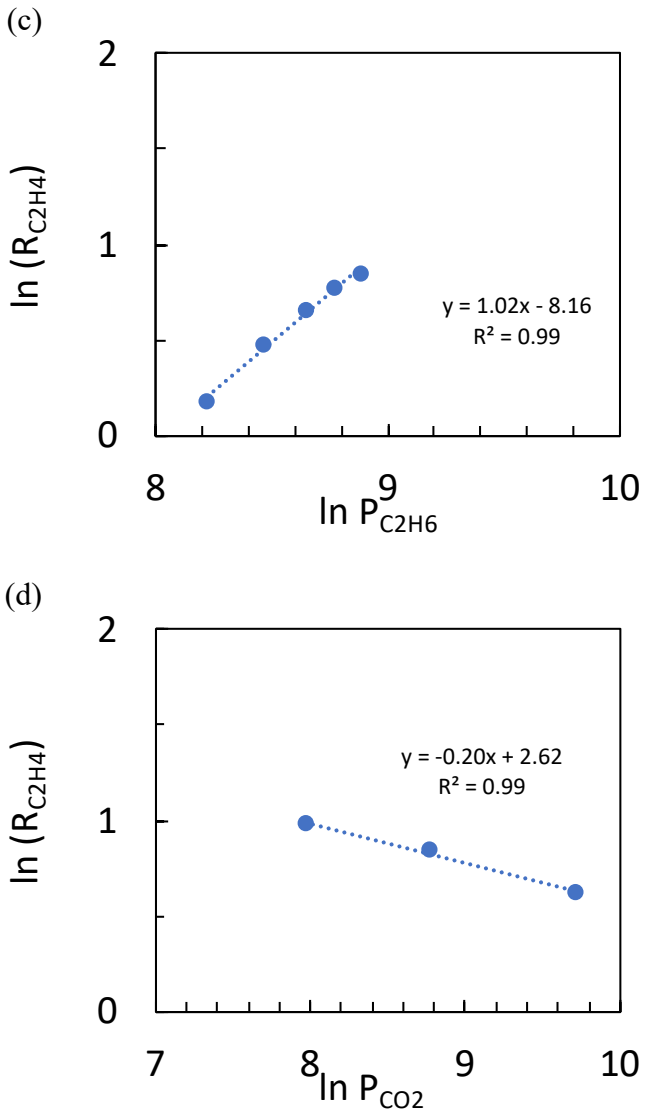

Figure B- 3: Log-Log plot of a) rate of C_2H_6 consumption, b) rate of C_2H_4 formation versus partial pressure of C_2H_6 and c) rate of C_2H_6 consumption, d) rate of C_2H_4 formation versus partial pressure of CO_2 to obtain reaction order using A15G1.

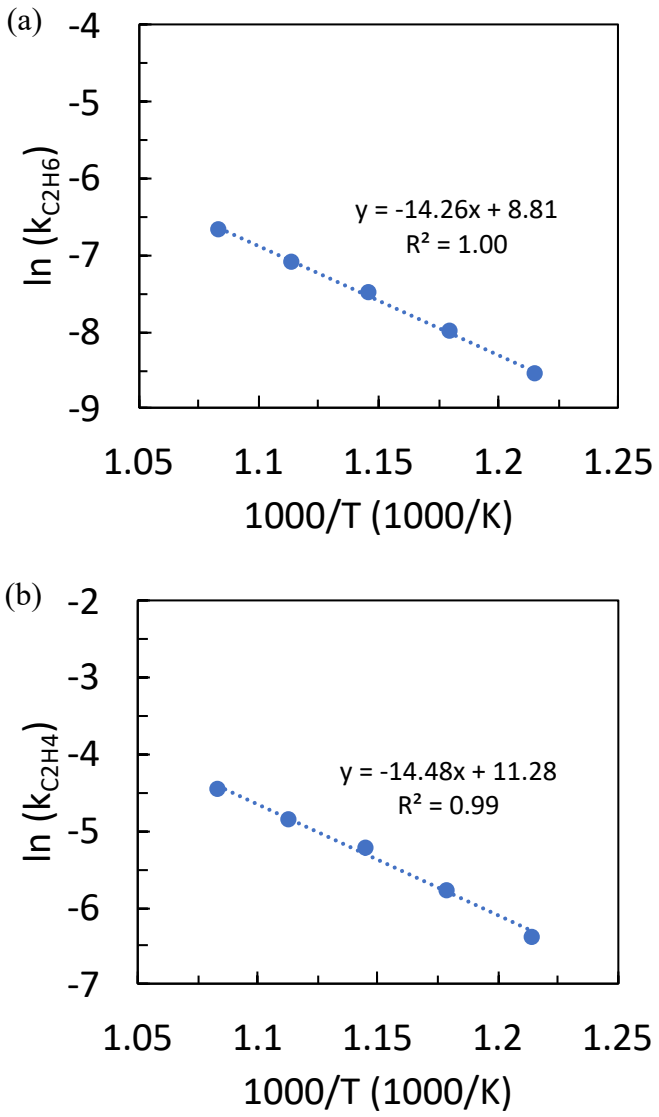

Figure B- 4: Arrhenius plot of a) C_2H_6 consumption and b) of C_2H_4 using A15G1.

(a)

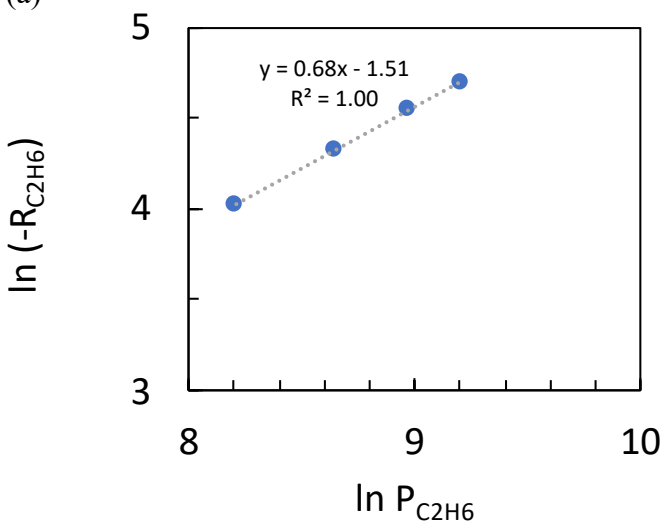
y = 0.68x - 1.51
R² = 1.00
5
4
3
8
9
10
ln (-R_C2H6)
ln P_C2H6

(b)

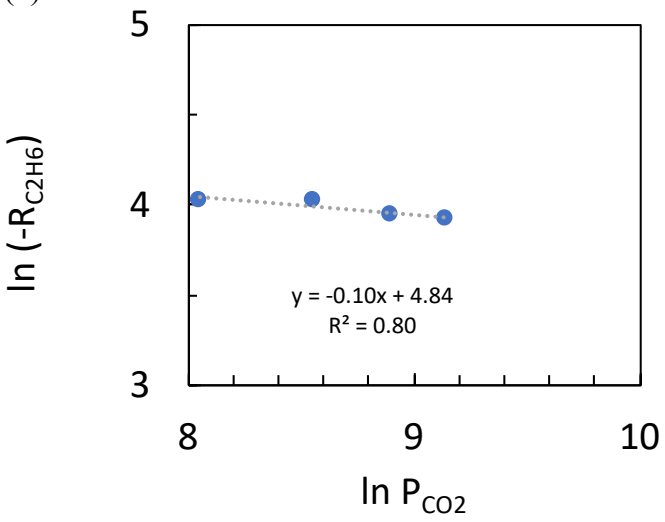
y = -0.10x + 4.84
R² = 0.80
5
4
3
8
9
10
ln (-R_C2H6)
ln P_CO2

(c)

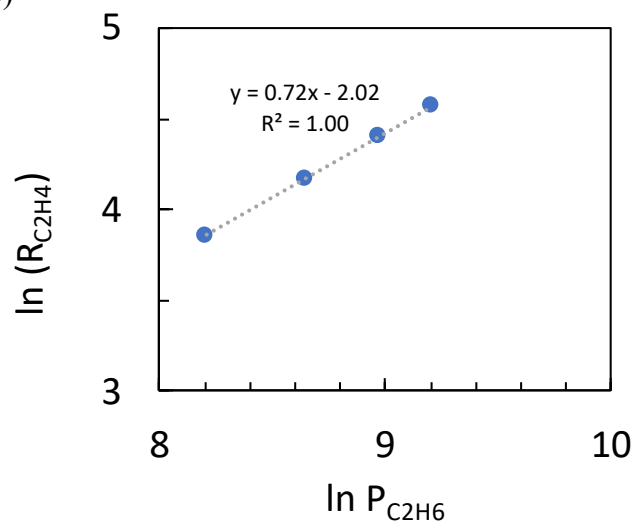

(d)

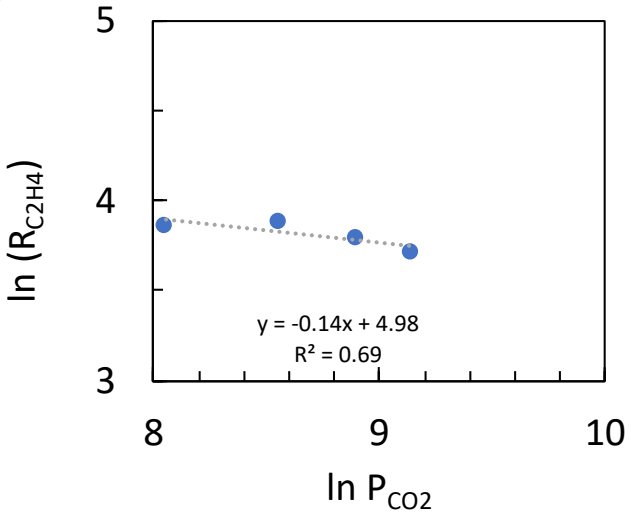

Figure B- 5: Log-Log plot of a) rate of C_2H_6 consumption, b) rate of C_2H_4 formation versus partial pressure of C_2H_6 and c) rate of C_2H_6 consumption, d) rate of C_2H_4 formation versus partial pressure of CO_2 to obtain reaction order using A5G1.

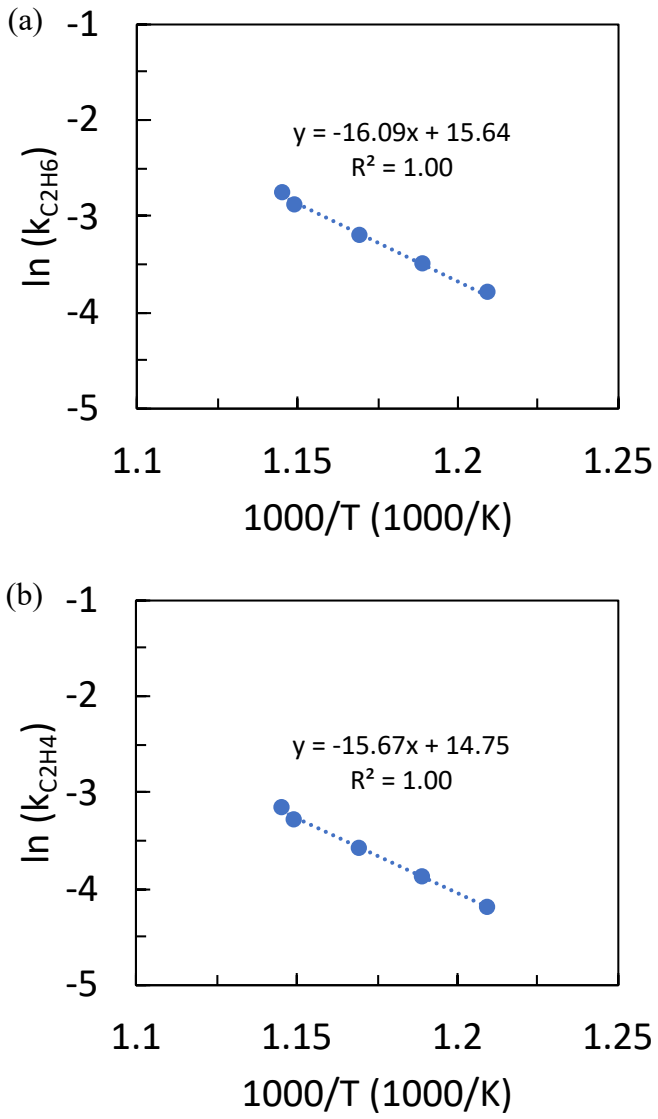

Figure B- 6: Arrhenius plot of a) C_2H_6 consumption and b) of C_2H_4 using A5G1.

(a)

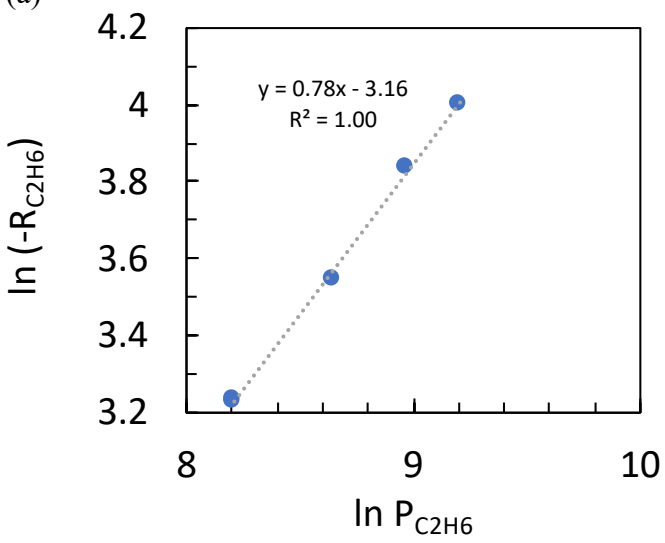
y = 0.78x - 3.16
R² = 1.00
4.2
4
3.8
3.6
3.4
3.2
8
9
10
ln (-R_C2H6)
ln P_C2H6

(b)

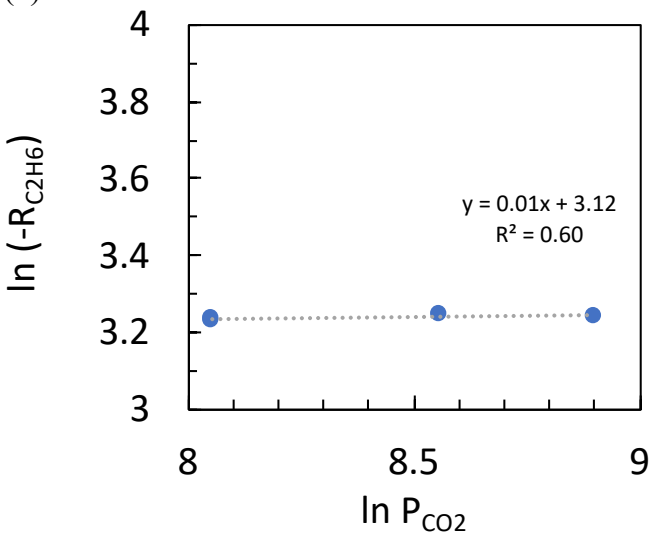
y = 0.01x + 3.12
R² = 0.60
4
3.8
3.6
3.4
3.2
3
8
8.5
9
ln (-R_C2H6)
ln P_CO2

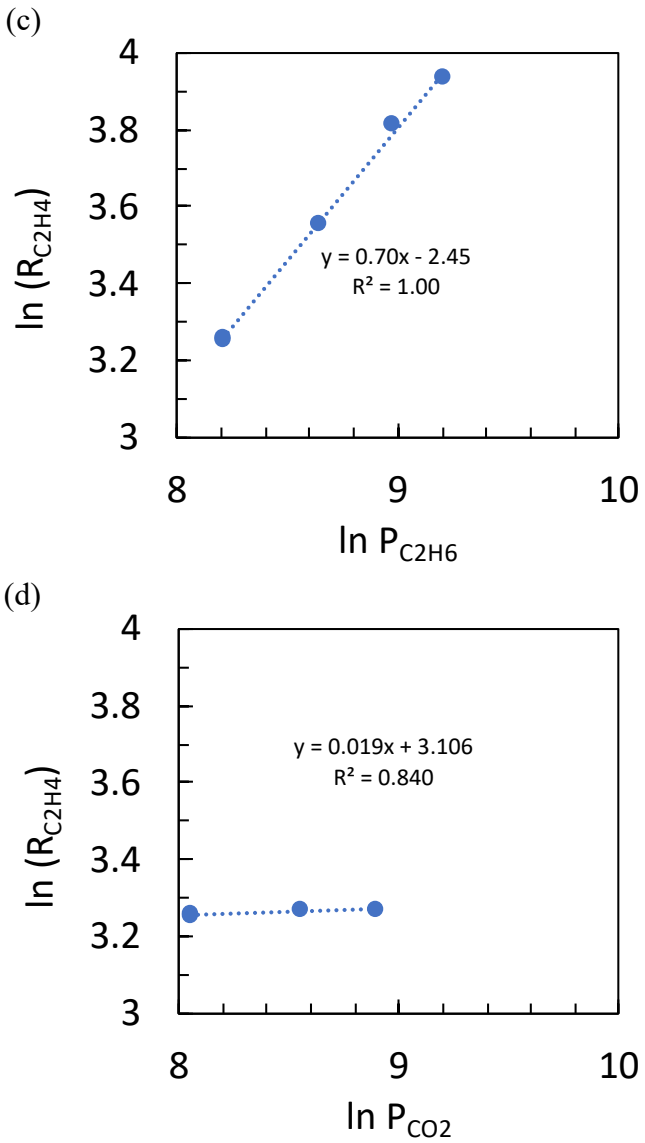

Figure B- 7: Log-Log plot of a) rate of C_2H_6 consumption, b) rate of C_2H_4 formation versus partial pressure of C_2H_6 and c) rate of C_2H_6 consumption, d) rate of C_2H_4 formation versus partial pressure of CO_2 to obtain reaction order using Ga_2O_3.

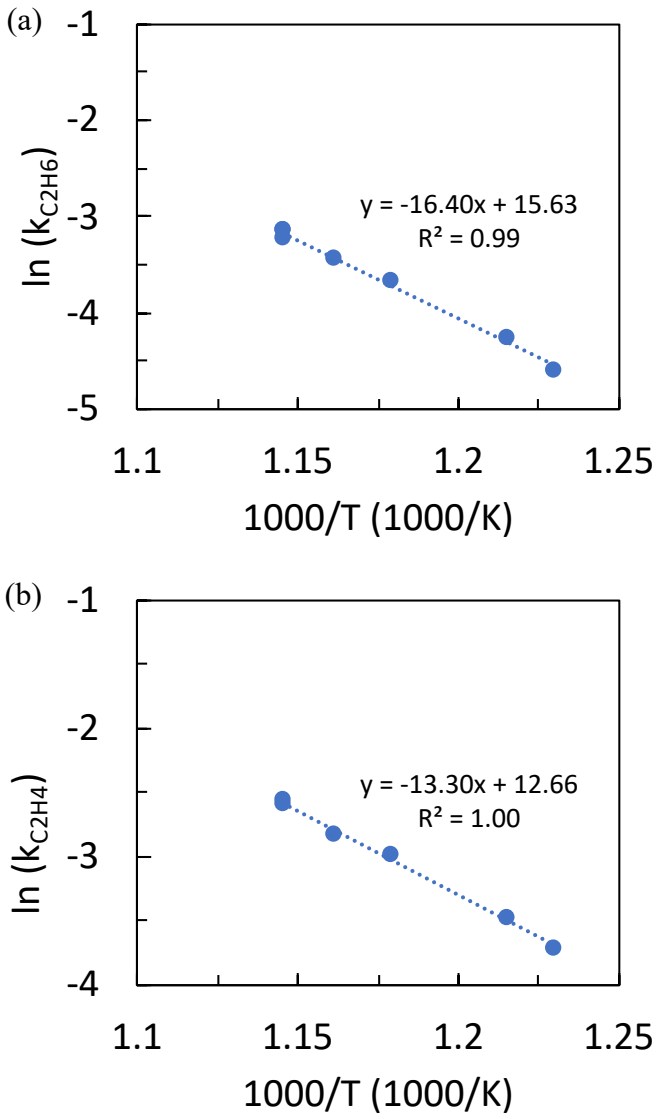

Figure B- 8: Arrhenius plot of a) C_2H_6 consumption and b) of C_2H_4 using Ga_2O_3.

Appendix C

The Deconvolution of C1s Scan Spectra from XPS

Table A- 1 The fitting constrains added on the deconvolution of C1s spectrum

	sp2	sp3	C-O	C=O	COO	Carbonate
Position Constrain (eV)	A (284.5 284.3)	A + 0.4	A+1.8	A+3	A+4.3	A+5.1
FWHM Constrain (eV)	A (0.2 5)	A*1	A*1	A*1	A*1	A*1

The constrains are added on position and peak width for the deconvolution of the C1s spectrum into the spectra of different carbon material species.

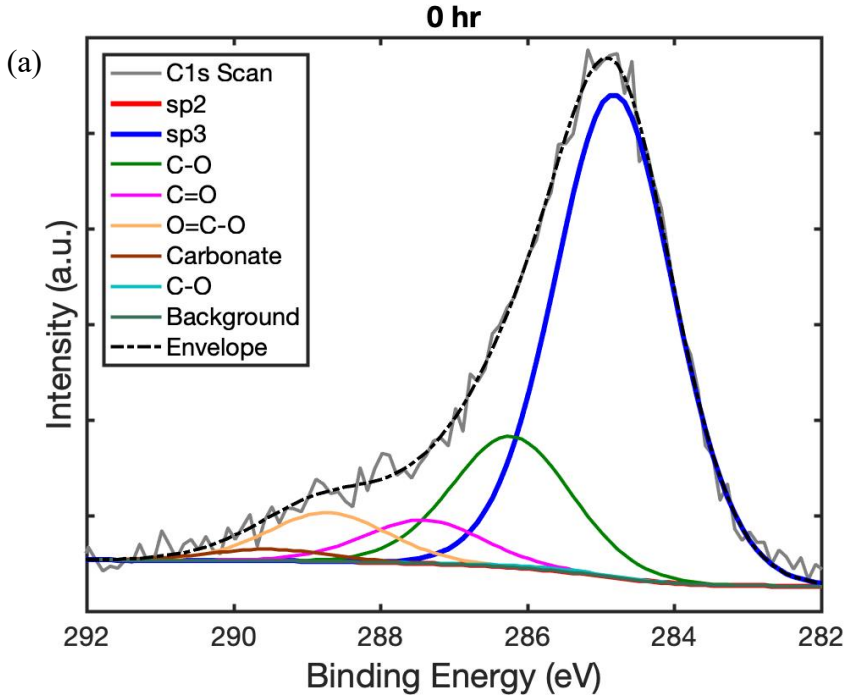

(b)

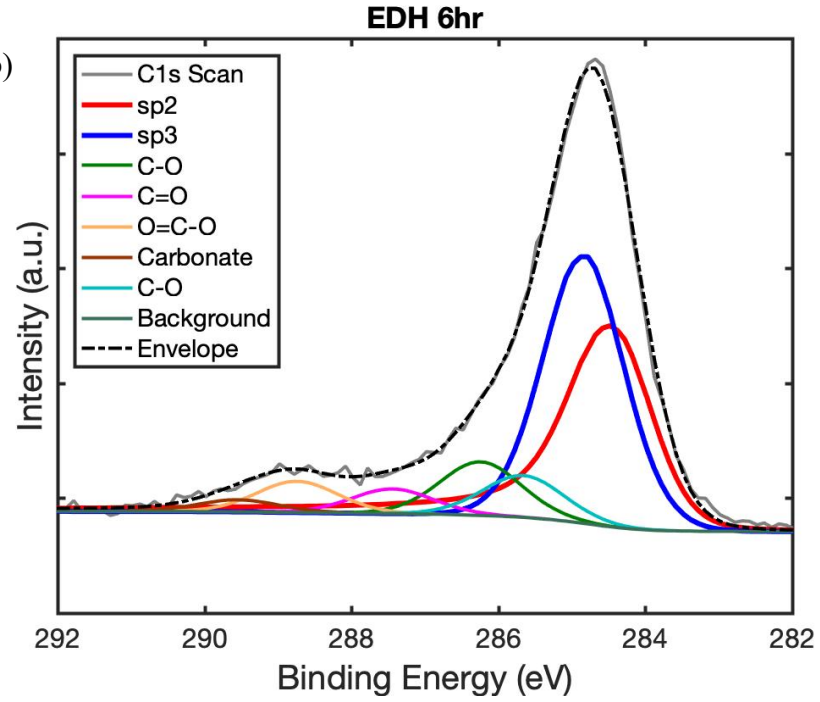
EDH 6hr
C1s Scan
sp2
sp3
C-O
C=O
O=C-O
Carbonate
C-O
Background
Envelope
Intensity (a.u.)
292
290
288
286
284
282
Binding Energy (eV)

(c)

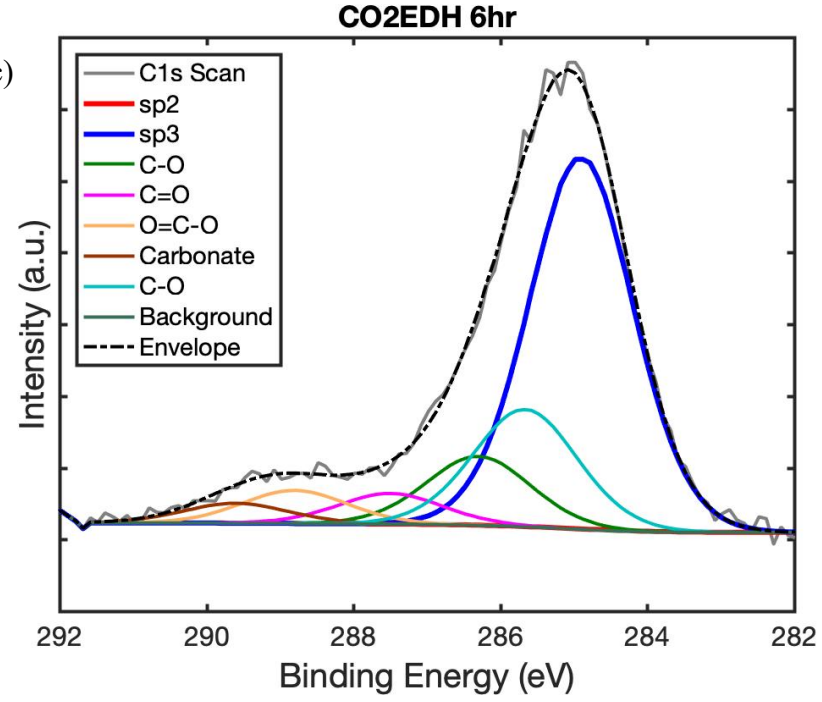
CO2EDH 6hr
C1s Scan
sp2
sp3
C-O
C=O
O=C-O
Carbonate
C-O
Background
Envelope
Intensity (a.u.)
292
290
288
286
284
282
Binding Energy (eV)

(d)

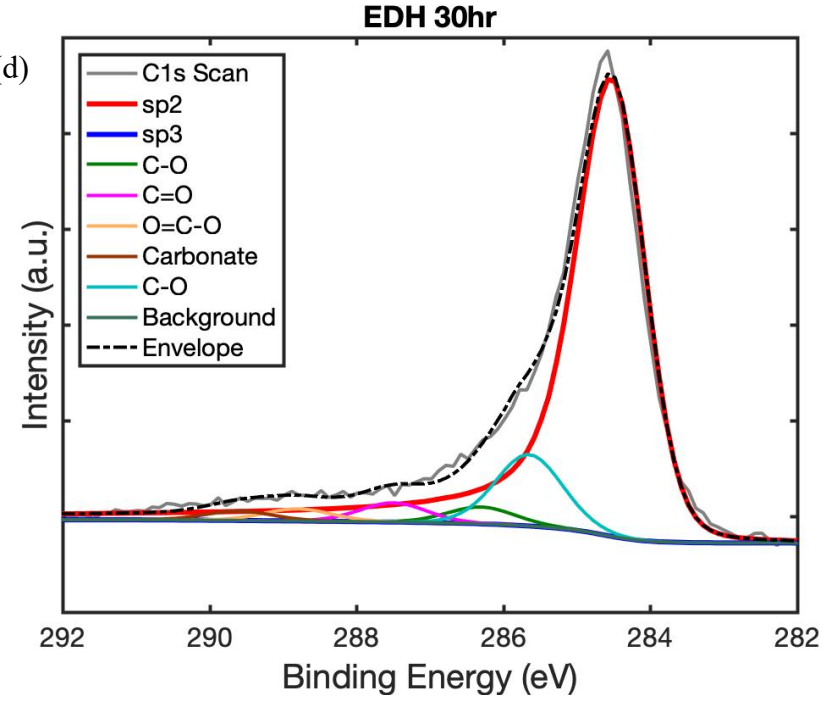
EDH 30hr
C1s Scan
sp2
sp3
C-O
C=O
O=C-O
Carbonate
C-O
Background
Envelope
Intensity (a.u.)
292
290
288
286
284
282
Binding Energy (eV)

(e)

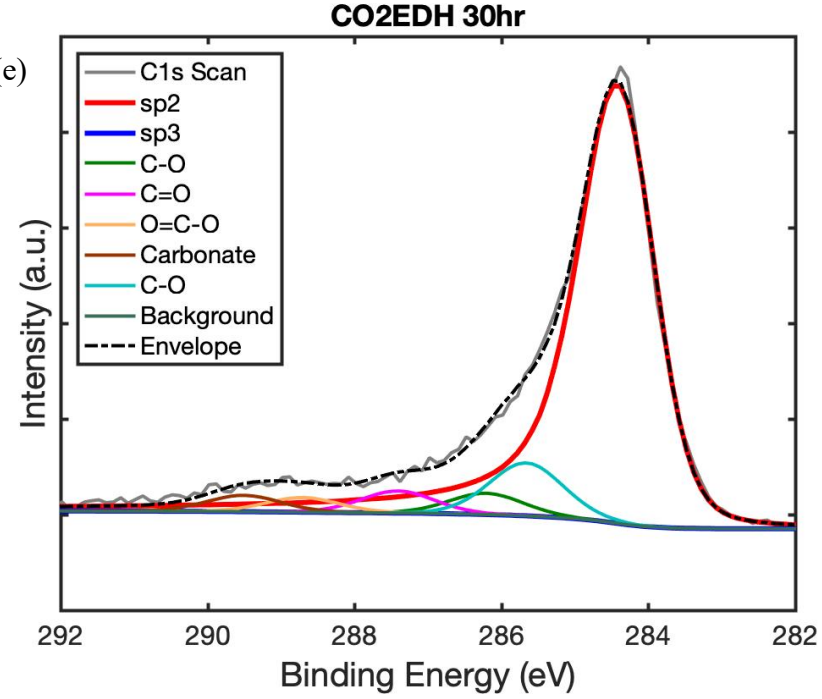
CO2EDH 30hr
C1s Scan
sp2
sp3
C-O
C=O
O=C-O
Carbonate
C-O
Background
Envelope
Intensity (a.u.)
292
290
288
286
284
282
Binding Energy (eV)

Figure C- 1: The deconvolution spectrum of C1s scan of the catalyst after (a) 0 hr reaction (fresh catalyst), (b) 6 hr EDH, (c) 6 hr CO2EDH, (d) 30 hr EDH and (e) 30 hr CO2EDH.